Component sizing and energy management for SOFC-based ship power systems

Haseltalab, Ali; van Biert, Lindert; Sapra, Harsh; Mestemaker, Benny; Negenborn, Rudy R.

DOI
10.1016/j.enconman.2021.114625

Publication date
2021

Document Version
Final published version

Published in
Energy Conversion and Management

Citation (APA)
Haseltalab, A., van Biert, L., Sapra, H., Mestemaker, B., & Negenborn, R. R. (2021). Component sizing and energy management for SOFC-based ship power systems. *Energy Conversion and Management*, *245*, Article 114625. https://doi.org/10.1016/j.enconman.2021.114625

Energy Conversion and Management 245 (2021) 114625

Contents lists available at ScienceDirect

Energy Conversion and Management

journal homepage: www.elsevier.com/locate/enconman

Component sizing and energy management for SOFC-based ship power systems

Ali Haseltalab [a,*], Lindert van Biert [a], Harsh Sapra [a], Benny Mestemaker [b], Rudy R. Negenborn [a]

[a] Deprtment of Maritime and Transport Technology, Delft University of Technology, Delft, the Netherlands
[b] Royal IHC, the Netherlands

ARTICLE INFO

Keywords:
Hybrid power generation
Solid oxide fuel cells
Energy management
Power and propulsion systems
Gas engine
Battery

ABSTRACT

The shipping industry is facing increasing demands to reduce its environmental footprints. This has resulted in adoption of new and more environmental friendly power sources and fuels for on-board power generation. One of these novel power sources is the Solid Oxide Fuel Cell (SOFC) which has a great potential to act as a power source, thanks to its high efficiency and capability to handle a wide variety of fuel types. However, SOFCs suffer from low transient capabilities and therefore have never been considered to be used as the main power source for maritime applications. In this paper, novel component sizing, energy and power management approaches are proposed to enable the use of SOFCs as the main on-board power source for the first time in the literature and integrate them into the liquefied natural gas fueled Power and Propulsion System (PPS) of vessels. The proposed component sizing approach determines the power ratings of the on-board sources (SOFC, gas engine and battery) considering size and weight limits, while the energy and power management approaches guarantee an optimal power split between different power sources and PPS stability while looking after battery aging. The results indicate that the combined proposed optimization-based approaches can yield up to 53% CO_2 reduction and 21% higher fuel utilization efficiency compared to conventional diesel-electric vessels.

1. Introduction

The stringent demands by the national and international authorities to reduce the environmental footprints of the shipping industry have pushed the industry towards the use and adoption of cleaner power sources as well as alternative fuels. As a result, it is expected that the emissions of hazardous pollutants, including sulphurous oxides, Nitrous Oxides (NO_x), particulate matter, and greenhouse gases will decrease drastically in the coming years [1]. Liquefied Natural Gas (LNG) is one of the alternative fuels that is being considered as a transition fuel towards zero-emission transport by the shipping industry. LNG results in less emissions of sulfur, particulate matter, and NO_x [2]. It also fulfills the current stringent sulphur regulations.

LNG can be used as a fuel in natural gas engines and Solid Oxide Fuel Cells (SOFC), where the later has an average 15% higher efficiency and very little NO_x and particular matter emissions. However, SOFCs have very low power transient capabilities compared to conventional diesel engines, which makes them hard to integrate into the ship Power and Propulsion Systems (PPS) [3]. Although, gas engines have faster transient capabilities than SOFCs, they are still slower than diesel engines. As a result, the use of SOFCs (and also pure gas engines) in vessels with fast load variations is challenging. These energy sources are mostly pared with batteries in the maritime and automotive industry [3,4], where the SOFC is normally used for generating the so-called base load, that is the minimum required load during the operation, and the engine and the battery act as principal and auxiliary sources [5]. Due to this limitation and the lower power density of SOFCs in comparison to engines, their share in the total installed power on-board is usually limited.

The combination of SOFC, gas engine, and battery requires advanced PPS configurations due to the nature of these energy sources. One of the most advanced and efficient PPS that is considered by the maritime industry, is the all-electric Direct Current (DC)-PPS [6,7]. Due to the DC interface of SOFC and battery, a DC-PPS is an appropriate candidate for the integration of SOFCs and batteries. However, because of the major difference in dynamics and efficiency characteristics of gas engine, SOFC, and battery, enabling this complex PPS with these novel energy sources is a difficult challenge.

* Corresponding author.
E-mail addresses: a.haseltalab@tudelft.nl (A. Haseltalab), l.vanbiert@tudelft.nl (L. van Biert), h.d.sapra@tudelft.nl (H. Sapra), r.r.negenborn@tudelft.nl (B. Mestemaker), btw.mestemaker@royalihc.com (R.R. Negenborn).

https://doi.org/10.1016/j.enconman.2021.114625
Received 31 May 2021; Accepted 8 August 2021
Available online 19 August 2021

1.1. Literature review

Fuel cells are currently being considered for maritime applications in order to achieve a 50% reduction of greenhouse gas emissions by 2050 [8]. Among the different types of fuel cells, Proton Exchange Membrane Fuel Cells (PEMFC) and SOFCs are considered as the most promising technologies [3]. While PEMFCs have higher power densities compared to SOFCs and behave better facing dynamical operating profiles, the preference for purified hydrogen fueling makes them less favorable for maritime applications as considerable storage volumes are required [9]. In contrast, high temperature SOFCs can generate electric power efficiently from various fuels, including LNG. As a result SOFCs are a potential fuel cell technology for medium to long distance ship applications [10].

PEMFCs are considered for some ship types including ferries and inland vessels, due to the higher maturity in mobile applications [4,11]. Maritime application of SOFCs has been studied in various research projects as well. An SOFC-gas turbine combined system generating electricity, heat and cooling was studied in the FELICITAS project [12]. In the METHAPU project, a 20 kW methanol-fuelled SOFC system was demonstrated on the RoRo carrier Wallenius Wilhelmsen [13,14]. This demonstration was complemented with a life cycle analysis and a conceptual design of an offshore supply vessel [15,16]. Methanol-fuelled SOFCs are studied in [17,18] as an auxiliary on-board power source.

A diesel–fueled SOFC system was developed in the SchIBZ project, demonstrating an efficiency up to 55% [19,20]. SOFCs have been considered by the US navy for underwater applications, where the SOFC is in charge of generating power for low speed cruising and a gas turbine generates the power required for higher speeds [21,22]. SOFCs are also suggested as an auxiliary on-board power source [23]. In [24], a 120 kW diesel–fuelled SOFC is considered and thermodynamically analysed for a naval vessel with the aim increasing the overall system fuel efficiency.

Dynamic modelling of a hybrid SOFC-Engine system is carried out in [25], where it is shown that slow dynamics of the SOFC dominates the overall performance of the power system. A novel SOFC-Engine integration approach is proposed in [26], where significant efficiency and emission reductions over traditional systems are shown. The authors also claim that using this integration methodology, a power split favouring the engine may be more beneficial. In [27], a hybrid plant based on diesel engine and methane fuelled SOFCs is proposed for an offshore support vessel where the fuel cells are used during slow cruising operations and have around four times less power output compared to the 2.4 MW utilised engine. The PPS configuration proposed in [28] also mainly relies on the engines, while the SOFC is used to provide a part of the hotel load as well as potentially some propulsive power. In order to deal with transients loads. an SOFC is considered together with a gas turbine in [29], where the SOFC provides a base load and the gas turbine carries out the load following.

Energy management for hybrid power generation on-board is studied extensively, as it is shown that the complexity of novel hybrid [30] and all-electric [6,31] PPS requires the adoption of advanced control and energy management approaches [32]. In this regard, most of the research works have been on the combination engine and battery with [33] or without [6] shore charging. Recently, maritime researchers have shifted their focus towards energy management for hybrid power generation using fuel cells. Most of these works focus on the integration of PEMFCs into the PPS. In [34], four different energy management approaches are proposed for different operating modes of a fully electric ferry where a PEMFC and a battery are the main energy sources. In [35], a cost minimising energy management approach is proposed for a similar fully electric PPS configuration where reinforcement learning approaches are used to overcome uncertainties in the operating profile. Similar approaches are also used in [36] to achieve the optimal split between battery and the fuel cell. Sizing optimization of the battery, supercapacitors, and battery based on the energy management approach is studied in [37], with the aim of improving operational performance and efficiency. PEMFCs have much faster load transients and need hybridization with batteries only to prevent high current ramps and unnecessary shut downs as these are detrimental for their lifetime.

Although energy management approaches have been studies extensively for small, fully electric vessels with PEMFCs and batteries on-board, it has hardly been studied for ships with SOFCs on-board [10]. On the other hand, the design of novel energy and power management approaches for SOFC-powered vehicles has started recently in the automotive industry, where the SOFC is used as an auxiliary or a secondary power source [38,39].

1.2. Research gaps and contributions of the paper

The integration of SOFCs into the PPS has recently gained attention, but the energy and power management for such a hybrid power generation system has not been studied before. Most of the works on the integration of SOFCs have mainly considered the efficiency from the design point of view, and as a result, energy management and component sizing, and design have never been studied hand in hand [10]. Moreover, in almost all of the proposed SOFC-integrated PPS designs, the fuel cell is used as an auxiliary or the secondary power source due to its slow transient capabilities, low specific power and limited power density. This leads to small efficiency gains and the necessity to use diesel fueled engines which results either in carrying two types of fuels (for example diesel and natural gas) or relatively high emissions.

Dynamic and static modeling of the overall SOFC-integrated PPS has also rarely been studied. The complexity of such a hybrid system where a variety of power sources with different characteristics are taken on-board, calls for a detailed analysis. This study will lead to the proper choice of strategy for power management and guaranteeing the stability of the PPS.

Considering the above research gaps, in this paper, the aim is to study design, modeling, energy and power management for hybrid power generation using SOFCs hand in hand. In this regard, first the PPS is considered where a DC-PPS architecture is proposed in which LNG is the only fuel on-board and SOFC, gas engine and a battery are the power sources. Mathematical models are given for the main components of this DC-PPS and are combined to create the overall state-space model of the on-board power system. Using this model, transient capabilities of power sources are studied and a power management approach is proposed.

An optimization-based energy management approach is proposed to guarantee the optimal power split between different energy sources on-board in which SOFC can act as the main energy source. The battery is used to shave peak powers and keep up with the fast load transients. To enable such a strategy, a moving window averaging technique is adopted, which acts as a mid-pass filter and calculates the average of real-time required power over a bounded time window. Therefore, the fast transients are removed and put aside to be handled by the battery. The time window size is determined using the transient capabilities of the slowest power sources on-board, in this case the SOFC. As a result, the SOFC and also the gas engine can keep up with the calculated mid-pass filter power output, which is higher than the base or the minimum required load, throughout the operation. The overall requested energy by the mid-pass filter is almost equal to the overall required energy during the operation, i.e., the SOFC can provide all of the required energy and there is no need for a gas engine if enough space and weight is available.

Based on the proposed energy management approach, a PPS optimization-based component sizing approach is presented in which the power and energy ratings of the on-board power are determined. In this design approach, space and weight limits act as constraints and maximized fuel efficiency is the objective. As a result, if the size and weight limitations are relaxed in the design stage, the DC-PPS can be established without a gas engine.

To evaluate the performance of the proposed component sizing,

energy and power management approaches, a dredging vessel is considered as an application case. This type of vessel has a highly varying and unpredictable load profiles which makes the overall control of the PPS challenging [40]. Real-life operating profiles are considered and validated models are used. The results show that the combination of the proposed schemes result in up to 32% CO_2 emissions reduction if the engine room size and weight remains unchanged and if the engine room size and weight is increased by 70% a switch to a fully SOFC powered DC-PPS can happen which results in 53% CO_2 emissions reduction compared to conventional diesel cases. The results show that for every percent increase of the engine room size, around 0.5% fuel consumption reduction can be achieved. Moreover, in comparison with fully gas engine-powered systems, the proposed approaches can decrease the CO_2 emissions by 40%, depending on the operating profile. More interestingly, using the proposed approaches, in case of retrofitting and availability of no extra space and weight, the energy generation efficiency is increased by 28% compared to the non–hybrid case. Furthermore, these results suggest that by the adoption of proposed approaches, the IMO emission reduction goals of 2030 can be achieved if the engine room size and weight limits are increased by 50%. With above 70% increase of the size and weight limits, the DC-PPS can be solely powered by SOFC which leads to 53% CO_2 reduction and 21% fuel utilization efficiency increase in comparison to conventional diesel-electric vessels.

All in all, the contributions of this paper are as follows:

1. Modeling and analysis of the SOFC-based all-electric PPS are under focus where a state-space model is proposed for the overall ship power system.
2. Energy and power management approaches are proposed which revolutionizes the SOFC-based hybrid power generation for maritime applications as they enable the SOFC to act as the main power source and supply most, even if no gas engine is required, all of the required operation energy.
3. Based on the presented energy management approach, an optimization-based component sizing scheme is proposed which aims at maximizing the fuel efficiency while satisfying the size and weight constraints.
4. This is the first paper that proposes energy and power management approaches for hybrid power generation using SOFCs on-board of vessels. It is also the first of its kinds in which the SOFCs are enabled to act as the main power source while the PPS can face varying and uncertain operating profiles.

1.3. Outline

The remainder of this paper is organized as follows. In Section 2, mathematical modeling of the DC-PPS components is carried out and then, a state space model is proposed for the overall system. In Section 3, proposed component sizing, energy and power management approaches are presented and discussed. In Section 4, simulation experiment results are presented. Concluding remarks and future research directions are given in Section 5.

2. Ship Power System Modeling

The DC-PPS for hybrid power generation using SOFCs is presented and described in this section. A DC-PPS can be divided into two (Fig. 1). The side which contains the power sources with their converters and rectifiers is called the power generation side while the side that contains the loads is called the power consumption side. In this PPS configuration, there is a gas engines, an SOFC and a battery on each side of the power generation side. The gas engine is connected to a synchronous generator which transforms the mechanical energy to electrical, and the synchronous generator is connected to a passive rectifier which turns the Alternative Current (AC) voltage to DC. The battery is connected to a bidirectional converter and the SOFC to a boost converter. The propulsion, dredging, and hotel loads are connected to the DC bus bar using motor controller inverters and DC to AC converters. The dynamics of these loads, represent a constant power load as shown in [41]. The focus this paper is on the power generation side for which, component sizing, energy and power management approaches are proposed to maximize efficiency and minimize emissions. In the remainder of this section, mathematical models are presented for different components of the power generation side and then by putting the models together a mathematical model for the overall power system is created.

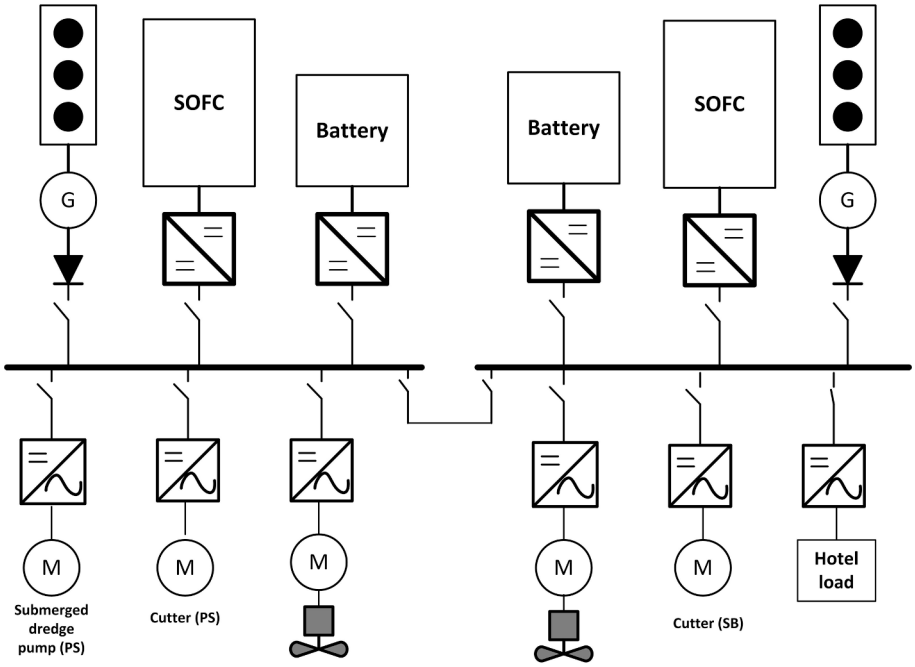

Fig. 1. The DC-PPS under study. The power generation side comprises gas engine-generator sets, SOFCs and batteries and the loads are on the power consumption side.

2.1. Engine

The gas engine is a power supplier which transforms chemical energy to mechanical energy. The power produced in the DC-PPS configuration appears as torque generation in a constant or variable speed. The engine dynamics can be approximated by nonlinear or linear equations (see, e.g., [42,43,30]), depending on the level of accuracy required for the study. In this paper, a linear model is adopted to accommodate the relationship between the fuel index and produced torque Q_{en} by means of a dynamical equation as below [44]:

$$\dot{Q}_{ge}(t) = -\frac{1}{\tau_{ge}}\left(Q_{ge}(t) + K_{ge} f_{ge}(t)\right), \tag{1}$$

where K_{ge} is the torque constant, f_{ge} is the governor setting (i.e., fuel index and flow) and τ_{ge} is the torque buildup constant which determines the response speed of the engine.

The gas engine transients are also controlled by a rate limiter which is designed based on the product guide of the considered engine. The adoption of this limiter is necessary as real engines should be loaded and unloaded based on their physical characteristics and capabilities. In Fig. 2, the maximum possible loading rate of a dual fuel engine is shown.

2.2. Synchronous generator

The Park equivalent Direct-Quadratic (dq) modeling approach is used to represent the dynamics of the synchronous generator. The relationship between the voltages, fluxes, and currents in the dq reference frame is established using the following equations:

$$\begin{aligned}\dot{\psi}_d(t) &= -v_d(t) + \frac{\omega_{ge}(t)\psi_q(t)}{g_r} + r_s i_d(t)\dot{\psi}_q(t)\\ &= -v_q(t) + \frac{\omega_{ge}(t)\psi_d(t)}{g_r} + r_s i_q(t)\dot{\psi}_{fd}(t) = v_{fd}(t) - r_{fd} i_{fd}(t)\dot{\psi}_{kd}(t)\\ &= -r_{kd} i_{kd}(t)\dot{\psi}_{kq}(t) = -r_{kq} i_{kq}(t),\end{aligned} \tag{2}$$

where r_s, r_{fd}, r_{kd}, and r_{kq} are stator, field circuit and damping resistances, respectively. Variables ψ_d and ψ_q are fluxes in the d and q axis, ψ_{kd} and ψ_{kq} are damping fluxes; the field flux is represented by ψ_{fd}. In the above model, v_d and v_q are dq voltages and v_{fd} is the field voltage of the generator. The mechanical dynamics of the synchronous generator are given as:

$$\dot{\omega}_{ge}(t = \frac{1}{2H}\left(\psi_d(t) i_q(t) - \psi_q(t) i_d(t) + g_r Q_{ge}(t)\right), \tag{3}$$

where ω_{ge} is the shaft speed of the engine-generator, Q_{ge} is the mechanical torque produced by the engine, g_r is the gear ratio between gas engine and generator, and $H = \frac{J}{p}$ is the inertia constant per pole. Using the system inductances, the relationship between electrical currents and fluxes can be established as:

$$I_G = \begin{bmatrix} i_d(t)\\ i_q(t)\\ i_{fd}(t)\\ i_{kd}(t)\\ i_{kq}(t)\end{bmatrix} = \begin{bmatrix} -L_d & 0 & L_{md} & L_{md} & 0\\ 0 & -L_q & 0 & 0 & L_{mq}\\ -L_{md} & 0 & L_{fd} & L_{md} & 0\\ -L_{md} & 0 & L_{md} & L_{kd} & 0\\ 0 & -L_{mq} & 0 & 0 & L_{kq}\end{bmatrix}^{-1} \begin{bmatrix} \psi_d(t)\\ \psi_q(t)\\ \psi_{fd}(t)\\ \psi_{kd}(t)\\ \psi_{kq}(t)\end{bmatrix}, \tag{4}$$

where $L_d, L_{md}, L_{kd}, L_{fd}, L_q, L_{mq}$ and L_{kq} are per unit inductances [46].

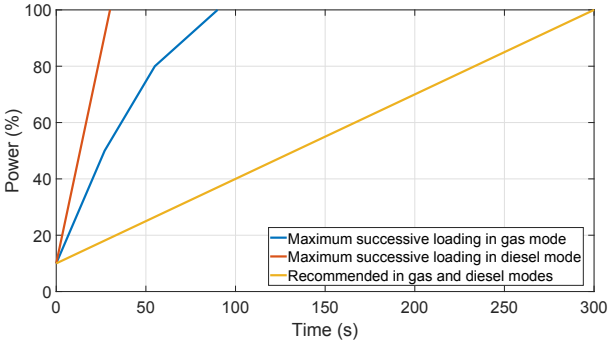

Fig. 2. Successive loading of Wärtsilä 34DF dual fuel engine series in gas and diesel modes [45].

2.3. Rectifier and the DC-link

The rectifier model is created using the generator's currents as input and DC current as the output. The DC current can be computed as:

$$i_{dc}(t) = \beta_{rec}\sqrt{i_q^2(t) + i_d^2(t)}. \tag{5}$$

The DC-link voltage is derived using the Kirchhoff equation:

$$\dot{v}_{dc}(t) = \frac{1}{C}\left(i_{dc}(t) - i_{load}(t)\right), \tag{6}$$

where i_{load} is the DC load current. Since, the ship loads resemble a constant power load, i_{load} can be defined as:

$$i_{load}(t) = \frac{P_{load}(t)}{v_{dc}(t)} \tag{7}$$

The dq-voltages from the rectifier to the generator are as follows:

$$v_q(t) = \alpha_{rec} v_{dc}(t)\cos\left(\theta_g(t)\right) v_d(t) = \alpha_{rec} v_{dc}(t)\sin\left(\theta_g(t)\right), \tag{8}$$

where θ_g is the load angle and is computed as below:

$$\theta_g(t) = \arctan\left(\frac{i_d(t)}{i_q(t)}\right) - \phi_{rec}. \tag{9}$$

Variables $\alpha_{rec}, \beta_{rec}$ and ϕ_{rec} are considered constant in this model.

For energy and power management studies, the efficiency and response time of the synchronous generator matters the most. In Fig. 3, the validation results for two different synchronous generators are given. The parameters of the other generators are built using the parameters of these two high voltage generators.

2.4. Battery

A model from [47] is used to represent the battery dynamics. This is suitable for power and energy management purposes. The dynamics in the change of the State-of-Charge (SoC) of the battery is determined using:

$$\dot{S_{oC}}(t) = -\left(\frac{\eta_i}{C_n}\right) i_b(t), \tag{10}$$

where η_i is the cell Coulombic efficiency, i.e., $\eta_i = 1$ for discharge and $\eta_i \leqslant 1$ for charge. Parameter C_n is the nominal capacity of the battery and i_b is the battery current. The battery voltage can be derived as:

$$v_b(t) = O_{CV}(S_{oC}(t)) - r_b i_b(t), \tag{11}$$

where O_{CV} is the open circuit voltage of the battery and is a function of S_{oC}. r_b is the battery resistance.

2.5. DC/DC converter

A non-isolated bidirectional converter is considered in this paper and its dynamical model is established using Kirchhoff current and voltage laws:

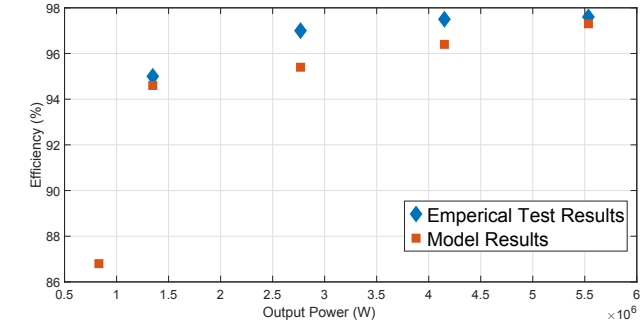

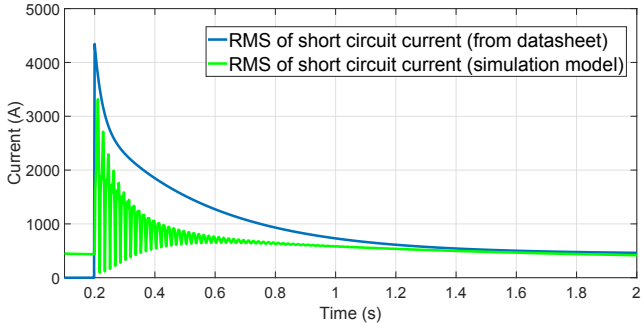

(a) 5.8 MW synchronous generator.

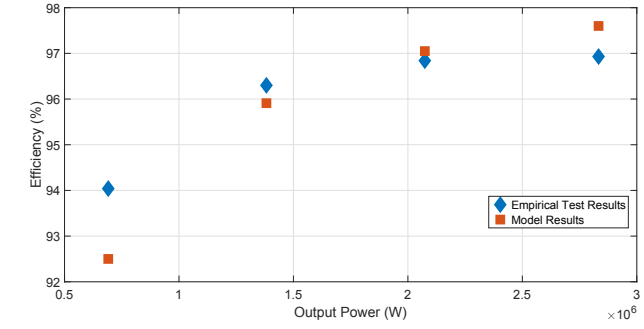

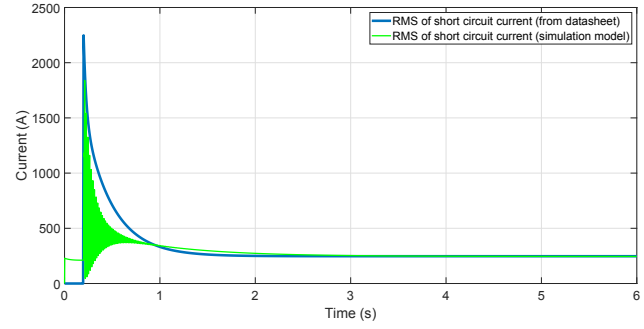

(b) 3.5 MW synchronous generator.

Fig. 3. Validation results of two synchronous generator sets. The parameters of these two generators are used to establish a model for other synchronous generators used.

$$\dot{i}_{\mathrm{Lb}}(t)=\frac{d_{\mathrm{bc}}(t)}{L_{\mathrm{bc}}}v_{\mathrm{dc}}(t)-\frac{v_{\mathrm{b}}(t)}{L_{\mathrm{bc}}}\dot{v}_{\mathrm{dc}}(t)=\frac{D_{\mathrm{bc}}}{C_{\mathrm{bc}}}i_{\mathrm{Lb}}(t)-\frac{i_{\mathrm{load}}(t)}{C_{\mathrm{bc}}},\tag{12}$$

where $d_{\mathrm{bc}}(t)$ is the duty cycle of the switching operation, i_{Lb} is the current of the equivalent inductor on the low voltage side of the converter, v_{b} is the battery voltage, L_{bc} is the inductance of the converter, and D_{bc} is the voltage ratio. A similar model is used for the SOFC converter, which only operates in the boost mode.

2.6. SOFC

A model is developed to calculate the current–voltage characteristics, fuel consumption for different loads and transient response of a typical SOFC system with internal reforming of natural gas. Such systems are described extensively in literature, for example by Ahmed et al. [48] and van Biert et al. [49]. The modelling equations are formulated such that the main dependencies are captured, while simplifying the simulation of thermal management and the power consumption of balance of plant components. Note that in this subsection t is omitted for the sake of notional simplicity.

Using an isothermal plug flow reactor model developed in [50], the electric power produced by the SOFC stack is calculated from:

$$P_{\mathrm{stack}}=i_{\mathrm{stack}}\cdot v_{\mathrm{stack}}=\frac{u_{\mathrm{f}}\cdot v_{\mathrm{cell}}\cdot A_{\mathrm{stack}}}{\int_0^{u_{\mathrm{f}}}d\vartheta/j(\vartheta)}\tag{13}$$

where u_f is the fuel fraction utilised in the stack, here assumed to be 0.85, $v_{\mathrm{cell}}=v_{\mathrm{stack}}/n_{\mathrm{series}}$ is the voltage produced by a single cell, j the local current density as a function of the electrochemical reaction coordinate ϑ, A_{stack} the total stack area and n_{series} the number of cells connected in series in each stack. The voltage produced by a single cells follows from [51]:

$$v_{\mathrm{cell}}=v_{\mathrm{Nernst}}(\vartheta)-\widehat{\eta}_{\mathrm{ohm}}(\vartheta)-\widehat{\eta}_{\mathrm{conc}}(\vartheta)-\widehat{\eta}_{\mathrm{act,an}}(\vartheta)-\widehat{\eta}_{\mathrm{act,ca}}(\vartheta),\tag{14}$$

where v_{Nernst} is the local Nernst potential and $\widehat{\eta}_{\mathrm{ohm}}$, $\widehat{\eta}_{\mathrm{conc}}$ and $\widehat{\eta}_{\mathrm{act}}$ are the ohmic, concentration and activation overpotentials respectively. The hydrogen oxidation reaction is assumed to dominate the electrochemistry, such that the local Nernst voltage follows from:

$$v_{\mathrm{Nernst}}(\vartheta)=-\frac{\Delta\overline{g}_{\mathrm{f}}}{2F}+\frac{\overline{R}T_{\mathrm{stack}}}{2F}ln\left\{\frac{\sqrt{y_{\mathrm{O_2}}(\vartheta)}\cdot y_{\mathrm{H_2}}(\vartheta)}{y_{\mathrm{H_2O}}(\vartheta)}\sqrt{\frac{p}{p_0}}\right\},\tag{15}$$

where $\Delta\overline{g}_{\mathrm{f}}$ is the Gibbs energy for hydrogen oxidation at standard pressure p_0 and average stack temperature T_{stack}, $\overline{R}$ the universal gas constant, F Faradays constant, p the actual pressure and y_i the local concentration of species i.

The concentrations of hydrogen and steam are calculated using Gibbs energy minimisation. The inlet composition is calculated assuming pure methane as a fuel, which is diluted with recirculated anode off-gas to reach an oxygen-to-carbon ratio of 2. The unburned fuel leaving the stack is combusted in an afterburner, and the hot flue gases are use to pre-heat and pre-reform fuel and air. Detailed calculations of such a system are shown in [50].

The ohmic overpotential follows from

$$\widehat{\eta}_{\mathrm{ohm}}(\vartheta)=j(\vartheta)\cdot\left(\frac{\tau_{\mathrm{an}}}{\sigma_{\mathrm{an}}}+\frac{\tau_{\mathrm{el}}}{\sigma_{\mathrm{el}}}+\frac{\tau_{\mathrm{ca}}}{\sigma_{\mathrm{ca}}}\right),\tag{16}$$

where τ and σ are the thickness and conductivity of the anode, electrolyte and cathode respectively. Since the SOFC is modelled as an isothermal reactor, the resistance is constant.

The concentration losses account for the deviation of the gas concentrations at the triple phase boundary from the bulk flow, mathematically expressed as:

$$\widehat{\eta}_{\mathrm{conc}}(\vartheta)=\frac{\overline{R}T_{\mathrm{stack}}}{2F}ln\left(\frac{p_{\mathrm{H_2O,tpb}}(\vartheta)\cdot p_{\mathrm{H_2}}(\vartheta)}{p_{\mathrm{H_2O}}(\vartheta)\cdot p_{\mathrm{H_2,tpb}}(\vartheta)}\right)+\frac{\overline{R}T_{\mathrm{stack}}}{4F}ln\left(\frac{p_{\mathrm{O_2}}(\vartheta)}{p_{\mathrm{O_2,tpb}}(\vartheta)}\right),\tag{17}$$

in which the reactant partial pressures at the triple phase boundary $p_{\mathrm{i,tpb}}$ depend on partial pressures in the bulk flow, stack temperature, effective diffusion coefficient and local current density:

$$p_{\mathrm{H_2,tpb}}(\vartheta)=p_{\mathrm{H_2}}(\vartheta)-\frac{\overline{R}T_{\mathrm{stack}}\tau_{\mathrm{an}}}{2FD_{\mathrm{eff,an}}}j(\vartheta),\tag{18}$$

$$p_{H_2O,tpb}(\vartheta) = p_{H_2O}(\vartheta) + \frac{\overline{R}T_{stack}\tau_{an}}{2FD_{eff,an}} j(\vartheta), \tag{19}$$

$$p_{O_2,tpb}(\vartheta) = p_{stack} - \left(p_{stack} - p_{O_2}(\vartheta)\right) exp\left(\frac{\overline{R}T_{stack}\tau_{ca}}{4FD_{eff,ca}p_{stack}} j(\vartheta)\right) \tag{20}$$

The activation overpotential losses in the anode are calculated from a corrected Butler–Volmer equation for the anode

$$j(\vartheta) = j_{0,an} \cdot \left[\frac{p_{H_2,tpb}(\vartheta)}{p_{H_2}(\vartheta)} exp\left(\frac{\omega 2F}{\overline{R}T_{stack}}\widehat{\eta}_{act,an}(\vartheta)\right) - \frac{p_{H_2O,tpb}(\vartheta)}{p_{H_2O}(\vartheta)} exp\left(-\frac{(1-\omega)2F}{\overline{R}T_{stack}}\widehat{\eta}_{act,an}(\vartheta)\right)\right], \tag{21}$$

where j_0 is the reference exchange current density and ω the symmetry factor. The exchange current density is a strong function of temperature, but treated as a constant due to the isothermal modelling assumption. The activation losses at the cathode are assumed to be dominated by charge transfer losses only:

$$j(\vartheta) = j_{0,ca} \cdot \left[exp\left(\frac{\omega 2F}{\overline{R}T_{stack}}\widehat{\eta}_{act,ca}(\vartheta)\right) - exp\left(-\frac{(1-\omega)2F}{\overline{R}T_{stack}}\widehat{\eta}_{act,ca}(\vartheta)\right)\right] \tag{22}$$

Eqs. (13)–(21), are solved to determine relations between stack power, cell voltage and current density. The stack area is calculated based on cell voltage at rated power (v_{cell} = 0.7 V). The cell voltage, stack voltage and current can be determined for the requested stack power based on these design conditions. Fig. 4 shows the cell voltage and normalised stack power versus normalised stack currents.

The model accounts for both constant losses independent of the load factor and load-dependent power consumption by the auxiliary system components to calculate the actual system power. For any requested SOFC system power, the corresponding stack power thus follows from:

$$P_{stack} = P_{sofc}\left(1 + P_{loss,ld}\right) + P_{loss,c}, \tag{23}$$

where P_{sofc} is the output power of the SOFC. A rate limiter τ_{SOFC} is applied to the stack current to comply with the typical operating limits imposed by SOFC system manufacturers [52]. The actual stack current is then used to calculate the actual voltage of the stack and the average voltage of a single cell.

The system efficiency, used to calculate the actual SOFC fuel consumption, subsequently follows from

$$\eta_{system} = \frac{P_{sofc}}{n_f \Delta h_f}, \tag{24}$$

with n_f the molar fuel flow at the system inlet.

An overview of the parameters used to model the SOFC system is given Appendix A which is based on typical operating characteristics reported by manufacturers.

2.7. The overall power system model

If all the power sources are connected, the dynamics of the DC-link can be represented as:

$$\dot{v}_{dc}(t) = \frac{1}{C}\left(\beta_{rec}\sqrt{I_G^T(t)G_2I_G(t)} + D_{bc}i_{Lb}(t) + D_{sofc}i_{stack}(t) - i_{load}(t)\right) \tag{25}$$

where D_{bc} and D_{sofc} are voltage ratios of battery and SOFC converters, respectively, $i_{load}(t) = \frac{P_{load}(t)}{v_{dc}(t)}$, and

$$G_1 = \begin{bmatrix} 1 & 0 & 0 & 0 & 0 \\ 0 & 1 & 0 & 0 & 0 \\ 0 & 0 & 0 & 0 & 0 \\ 0 & 0 & 0 & 0 & 0 \\ 0 & 0 & 0 & 0 & 0 \end{bmatrix}.$$

As a result, the overall dynamics of the energy generation side can be described using the following equations:

$$\begin{aligned} \dot{I}_G(t) &= X_G^{-1}S_\omega\left(\frac{\omega_{ge}(t)}{g_r}\right)X_GI_G(t) + X_G^{-1}R_GI_G(t) + v_{dc}(t)X_G^{-1}E \\ &\quad + X_G^{-1}bv_{fd}(t)\dot{\omega}_{ge}(t) \\ &= \frac{1}{2H}\left(Q_{ge}(t) - I_G^T(t)X_G^T(t)G_2I_G(t)\right)\dot{Q}_{ge}(t) \\ &= -\frac{Q_{ge}(t)}{\tau_s} + K_{ge}f_{ge}(t)\dot{i}_{Lb}(t) = \frac{d_{bc}(t)}{L_{bc}}v_{dc}(t) - \frac{v_b(t)}{L_{bc}}\dot{i}_{Lsofc}(t) \\ &= \frac{d_{sofc}(t)}{L_{sofc}}v_{dc}(t) - \frac{v_{stack}(t)}{L_{sofc}}\dot{v}_{dc}(t) \\ &= \frac{1}{C}\left(\beta_{rec}\sqrt{I_G^T(t)G_1I_G(t)} + D_{bc}i_{Lb}(t) + D_{sofc}i_{stack}(t) - \frac{P_{load}(t)}{v_{dc}(t)}\right) \end{aligned} \tag{26}$$

where

$$G_2 = \begin{bmatrix} 0 & 1 & 0 & 0 & 0 \\ -1 & 0 & 0 & 0 & 0 \\ 0 & 0 & 0 & 0 & 0 \\ 0 & 0 & 0 & 0 & 0 \\ 0 & 0 & 0 & 0 & 0 \end{bmatrix},$$

X_G is the matrix of inductances introduced in (4),

$$\begin{aligned} E_j &= \begin{bmatrix} \alpha_{rec_j}\sin\left(\arctan\left(\frac{i_{d_j}}{i_{q_j}}\right) - \phi_{rec_j}\right) \\ \alpha_{rec_j}\cos\left(\arctan\left(\frac{i_{d_j}}{i_{q_j}}\right) - \phi_{rec_j}\right) \\ 0 \\ 0 \\ 0 \end{bmatrix}, S_\omega\left(\frac{\omega_{ge}(t)}{g_r}\right) \\ &= \begin{bmatrix} 0 & \frac{\omega_{ge}(t)}{g_r} & 0 & 0 & 0 \\ \frac{\omega_{ge}(t)}{g_r} & 0 & 0 & 0 & 0 \\ 0 & 0 & 0 & 0 & 0 \\ 0 & 0 & 0 & 0 & 0 \\ 0 & 0 & 0 & 0 & 0 \end{bmatrix} \end{aligned} \tag{27}$$

and the matrix of resistances is:

$$R_G = \begin{bmatrix} r_s & 0 & 0 & 0 & 0 \\ 0 & r_s & 0 & 0 & 0 \\ 0 & 0 & -r_{fd} & 0 & 0 \\ 0 & 0 & 0 & -r_{kd} & 0 \\ 0 & 0 & 0 & 0 & -r_{kq} \end{bmatrix}. \tag{28}$$

In the next section, component sizing, energy and power management approaches are introduced for the DC-PPS system presented in this section.

3. Proposed Component Sizing, Energy and Power Management Approaches

In this section, the proposed approaches for the power system component sizing, energy management, and power management are

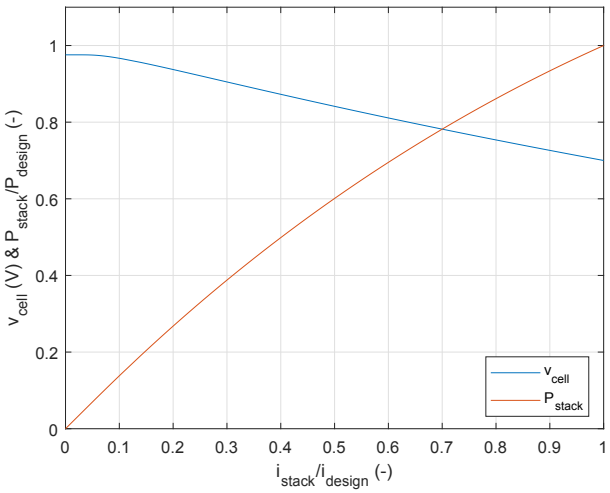

Fig. 4. Schematic overview of the simplified method used to estimate the cell potential from the reversible potential r_{rev}, voltage loss at open circuit Δv_{OC}, stack current i_{stack} and equivalent cell resistance r_{eq}.

presented. The power system component sizing approach aims at enabling maximum fuel efficiency during operation by optimizing the power source sizes based on the weight and space limits. During the operation, the energy management module solves an optimization problem at each sampling time to find the optimal power split between different on-board sources. The power management module consists of a group of controllers which control the voltages and currents of the power system as well as the shaft speed of the engine-synchronous generator set. While the component sizing approach is utilized for the ship design stage, the energy and power management approaches are used during the operation. However, the proposed optimization-based component sizing approach is created based on the philosophy behind the energy management approach.

A median pass filter is designed for the energy management module, which works based on the moving average window principle. The filter takes the average of the required load over a bounded time window. As a result, the output of this filter has slower transient which is suitable for the SOFC and also the gas engine. It reaches way higher values compared to the minimum required or the base load. The size of this window is determined based on the transient capabilities of the SOFC and the gas engine. Therefore, the power output of the SOFC and engine together should be as much as the maximum value of the filter output. In Fig. 5, an operating profile of a dredger is shown. This median filtering technique is first explained in the remainder of this section, after which the proposed component sizing, energy and power management approaches are presented.

3.1. The moving average filter

Suppose $P_{load}(k)$ is the overall load power at discrete time instant k. Variable $P_{load}(k)$ is bounded, i.e., $P_{load}(k) \in [0, P_{max}]$. If the duration between two consecutive sampling times is Δk, then, the overall energy required for the operation is:

$$E_{load}(N_e) = \Delta k \sum_{i=0}^{i=N_e} P_{load}(i), \tag{29}$$

where N_e is the end time of the operation. Using (29), the consumed energy in a bounded time window N_w can be calculated as:

$$E_{load}(k) = \Delta k \sum_{i=k-N_w}^{i=k} P_{load}(i). \tag{30}$$

Note that, for all $P_{load}(i)$ with $i \leqslant 0$, $P_{load}(i) = 0$. Using the above

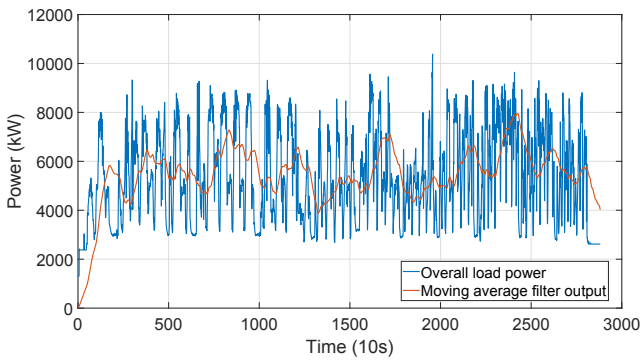

Fig. 5. Port side operating profile of a dredger versus the output of the moving average filter.

equation, the filter output that is the average of the required power at sampling time k over the time window N_w can be derived as:

$$\overline{P}_w(k) = \frac{1}{N_w} \sum_{i=k-N_w}^{i=k} P_{load}(i). \tag{31}$$

The size of N_w determines the transient speed of $\overline{P}_w$ over time, i.e., if $\Delta P_{w_{max}}$ is the maximum allowable difference between two consecutive filter outputs over time, we have:

$$|\overline{P}_w(k+1) - \overline{P}_w(k)| \leqslant \Delta P_{w_{max}}. \tag{32}$$

Using (31), the following inequality can be derived.

$$\frac{1}{N_w}|P_{load}(k+1) - P_{load}(k-N_w)| \leqslant \Delta P_{w_{max}}. \tag{33}$$

As a result, one can control the maximum magnitude of $\left|\overline{P}_w(k+1) - \overline{P}_w(k)\right|$ over time by changing the size of N_w.

3.2. The ship design approach: sizing of the power sources

In the design process of a vessel, numerous operating profiles that the vessel should be able to deal with are used. Each of these operating profiles resemble a bounded random signal. Moreover, if the moving average filter is also applied to this signal, its output, i.e., $\overline{P}_w(k)$ is also bounded and has a maximum value of $P_{w_{max}}$ that is $P_{w_{max}} \leqslant P_{max}$.

The proposed optimization-based component sizing approach is created based on the fuel efficiency of the gas engine and the SOFC. The battery size is determined based on the size of these two power sources and also the maximum required power. Assume $\eta_{max_{sofc}}$ and $\eta_{max_{GE}}$ are the full load Specific Fuel Consumption (SFC) values of SOFC and gas engine in g/kWh. The full load SFC $\eta_{max_{GE}}$ is more or less the same for engines with different power rantings that belong to the same manufacturing series (see [45] as an example). This is also the case for SOFCs. It is well known that the efficiency of SOFCs are higher than the efficiency engines [9].

The objective function of the component sizing optimization problem is established using $\eta_{max_{sofc}}$ and $\eta_{max_{GE}}$ as:

$$J_d\left(P_{\substack{max\\sofc}}, P_{\substack{max\\ge}}, P_{\substack{max\\b}}\right) = \eta_{max_{sofc}} P_{\substack{max\\sofc}} + \eta_{max_{sofc}} P_{\substack{max\\ge}} + \eta_b P_{\substack{max\\b}} \tag{34}$$

where $P_{max_{sofc}}, P_{max_{ge}}$, and P_{max_b} are maximum deliverable power by the SOFC, engine, and the battery in kW, respectively. Parameter η_b is the charge efficiency of the battery in g/kWh using an engine and on the nominal C-rate.

Assume that the maximum available space and weight on-board of the vessel are denoted by S_v and W_v, respectively. Moreover, the volumetric power density (in m^3/kW) of the sources are shown with $d_{s_{sofc}}, d_{s_{ge}}$,

and d_{s_b}. The gravimetric power density (in tonne/kW) of the sources are denoted by $d_{w_{sofc}}$, $d_{w_{ge}}$, and d_{w_b}. The maximum possible charge and discharge C-rates of the battery is shown with $C_{rate_{max}}$. The weight and space constraints are defined respectively as:

$$0 \leqslant d_{w_{sofc}} P^{max}_{sofc} + d_{w_{ge}} P^{max}_{ge} + d_{w_b} \frac{P^{max}_{b}}{C_{rate_{max}}} \leqslant W_v 0 \leqslant d_{s_{sofc}} P^{max}_{sofc} + d_{s_{ge}} P^{max}_{ge} + d_{s_b} \frac{P^{max}_{b}}{C_{rate_{max}}} \leqslant S_v. \tag{35}$$

The objective function of the energy management problem can be established using the SFC functions in (39). The main objective of the energy management module is to minimize fuel consumption by finding the optimal split between different on-board power sources. As a result, the objective function at sampling time k is defined as:

$$J_{EM}\left(P_{sofc}(k), P_{ge}(k)\right) = P_{sofc}(k) S_{fc_{sofc}}\left(P_{sofc}(k)\right) + P_{ge}(k) S_{fc_{ge}}\left(P_{ge}(k)\right) = a_{sofc} P^2_{sofc}(k) + b_{sofc} P_{sofc}(k) + c_{sofc} + a_{ge} P^2_{ge}(k) + b_{ge} P_{ge}(k) + c_{ge}. \tag{40}$$

In the proposed component sizing and energy management approaches, the battery should be able to provide the power when the system faces loads with fast transient. Moreover, it has to be able to carry out peak shaving during an operating profile. Based on the principle of the moving average filtering, the battery should have a minimum capacity such that it can provide the extra required power and absorb the extra generated power. This capacity is a function of SOFC and gas engine transient capabilities. Suppose the minimum required time for SOFC and the gas engine to reach to their maximum possible power output from minimum power output (excluding the warm-up time) are denoted with $T_{rise_{sofc}}$ and $T_{rise_{ge}}$, respectively. Then, the constraint on the minimum required battery capacity is:

$$T_{rise_{sofc}} P^{max}_{sofc} + T_{rise_{ge}} P^{max}_{ge} \leqslant \frac{0.7 P^{max}_{b} T_{hr}}{C_{rate_{max}}} \tag{36}$$

which is established based on the maximum and minimum safe battery's SoC that are 90% and 20%, respectively [53,54]. In (36), $T_{hr} = 3600$s which accounts for an hour. The battery should be able to provide an equal amount of power as the SOFC and the gas engine together. Moreover, the combination of SOFC and engine should be able to provide power as much as $P_{w_{max}}$ and the combination of all power sources should be able to keep up with the maximum possible load P_{max}. These result in the following three constraints:

$$P^{max}_{sofc} + P^{max}_{ge} \leqslant P^{max}_{b} \quad P^{max}_{sofc} + P^{max}_{ge} \geqslant P_{w_{max}} \quad P^{max}_{sofc} + P^{max}_{ge} + P^{max}_{b} \leqslant P_{max}. \tag{37}$$

Using (34) and the defined constraints, the component sizing optimization problem can be established as:

$$\mathbb{P}_{design}: \min_{P^{max}_{sofc}, P^{max}_{ge}, P^{max}_{b}} J_d\left(P^{max}_{sofc}, P^{max}_{ge}, P^{max}_{b}\right) \tag{38}$$

subject to constraints in (35), (36), and (37).

3.3. The energy management approach

The energy management module works during the vessel's operation and its aim is to find the best power split between energy sources. The energy management optimization problem is established using the SFC curve of the SOFC and gas engine. The SFC curves of a SOFC and an engine can be defined as:

$$\begin{aligned} S_{fc_{sofc}}\left(P_{sofc}(t)\right) &= a_{sofc} P_{sofc}(t) + \frac{c_{sofc}}{P_{sofc}(t)} + b_{sofc} S_{fc_{ge}}\left(P_{ge}(t)\right) \\ &= a_{ge} P_{ge}(t) + \frac{c_{ge}}{P_{ge}(t)} + b_{ge} \end{aligned} \tag{39}$$

where $a_{sofc,ge}, b_{sofc,ge}$, and $c_{sofc,ge}$ are function coefficients and $P_{sofc}(t)$ and $P_{ge}(t)$ are the power of SOFC and gas engine at time t. The SFC curves of a SOFC and a gas engine are depicted in Fig. 6.

In the proposed energy management problem, SOFC and gas engine should provide the moving average load of the operating profile, i.e., the sum of SOFC and gas engine power should be equal to the output of the moving average filter, i.e.,

$$P_{sofc}(k) + P_{ge}(k) = \overline{P}_w(k). \tag{41}$$

Therefore, the transients of the filter should not be faster than the transients of the SOFC and engine, such that these power sources can keep up with the output of the moving average filter. To guarantee this, the window size of the moving average filter should be designed in accordance with the capabilities of the SOFC and the gas engine. As a result:

$$N_w = T_{rise_{sofc}} + T_{rise_{ge}}. \tag{42}$$

Eq. 42 is used in (31) to calculate the output of the moving average filter.

The constraints on the decision variables depend on the transient

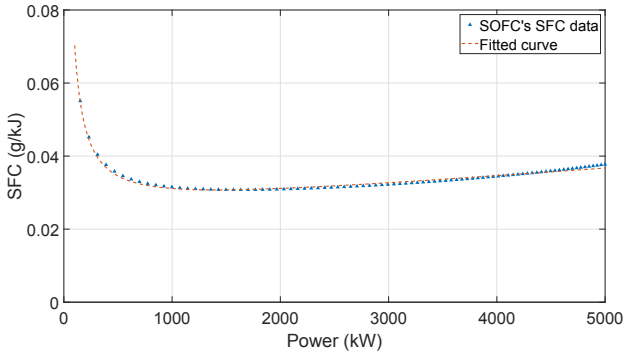

(a) SFC curve of a SOFC system.

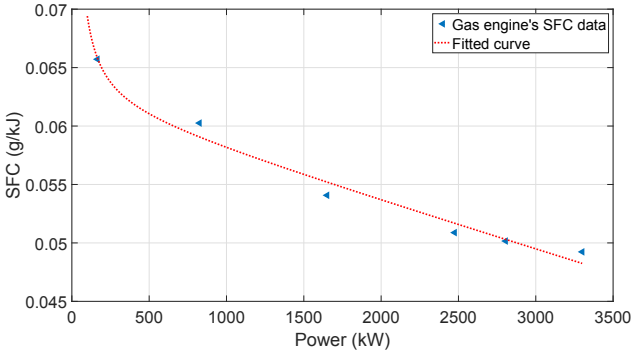

(b) SFC curve of a 3.3 MW gas engine [45].

Fig. 6. SFC curves of a SOFC and a gas engine versus the their SFC data.

capabilities of the power sources. These constraints can be defined as:

$$P_{\min_{\text{sofc}}} \leqslant P_{\text{sofc}}(k-1) - \Delta k \frac{P_{\max_{\text{sofc}}}}{T_{\text{rise}_{\text{sofc}}}} \leqslant P_{\text{sofc}}(k) \leqslant P_{\text{sofc}}(k-1) + \Delta k \frac{P_{\max_{\text{sofc}}}}{T_{\text{rise}_{\text{sofc}}}} \leqslant P_{\max_{\text{sofc}}} P_{\min_{\text{ge}}} \leqslant P_{\text{ge}}(k-1) - \Delta k \frac{P_{\max_{\text{ge}}}}{T_{\text{rise}_{\text{ge}}}} \leqslant P_{\text{ge}}(k) \leqslant P_{\text{ge}}(k-1) + \Delta k \frac{P_{\max_{\text{ge}}}}{T_{\text{rise}_{\text{ge}}}} \leqslant P_{\max_{\text{ge}}} \tag{43}$$

In the proposed energy management scheme, the battery takes the roll of peak shaver and keeps up with the fast transients. However, in order to maximize the life time of the battery and decrease the aging speed, the depth of discharge and average SoC should be controlled [55]. This can be done in optimization problem, but will lead to a nonlinear constraint due to the nonlinear relationship between battery's current i_{b} and power P_{b}. As a result, an alternative scheme is proposed in this section, that is:

if $S_{\text{oC}}(k-1) \leqslant S_{\text{oC}_{\min}}$ & $P_{\text{w}_{\max}} \geqslant P_{\text{load}}(k-1)$,

$$P'_{\text{load}}(k) = P_{\text{load}}(k) + \min\left(\frac{P_{\max_{\text{b}}}}{C_{\text{rate}_{\max}}}, P_{\text{w}_{\max}} - P_{\text{load}}(k-1)\right),$$

elseif $S_{\text{oC}}(k-1) \geqslant S_{\text{oC}_{\max}}$,

$$P'_{\text{load}}(k) = P_{\text{load}}(k) - \frac{P_{\max_{\text{b}}}}{C_{\text{rate}_{\max}}}$$

else,

$$P'_{\text{load}}(k) = P_{\text{load}}(k)$$

end

Then, the filter output is calculated as:

$$\overline{P}_{\text{w}}(k) = \frac{1}{N_{\text{w}}} \sum_{i=k-N_{\text{w}}}^{i=k} P_{\text{load}}{}'(i). \tag{44}$$

The energy management optimization problem can be defined as:

$$\mathbb{P}_{\text{EM}}: \min_{P_{\text{sofc}}(k), P_{\text{ge}}(k)} J_{\text{EM}}\left(P_{\text{sofc}}(k), P_{\text{ge}}(k)\right), \tag{45}$$

subject to the constraints in (41) and (43) and the battery power $P_{\text{b}}(k)$ is calculated as:

$$P_{\text{b}}(k) = P_{\text{load}}{}'(k) - P^*_{\text{sofc}}(k) - P^*_{\text{ge}}(k), \tag{46}$$

where P^*_{sofc} and P^*_{ge} are the outputs of the optimization problem.

3.4. The power management approach

In this part, an alternative approach to conventional droop control is proposed for controlling the on-board power sources in harmony with the energy management approach. It is shown that the conventional droop control approaches are insufficient for DC systems with different types of power sources [56]. This power management approach is designed based on the results in [41]. In the proposed DC-PPS, a passive six-pulse rectifier is used for the rectification stage and DC/DC converters for the SOFC and battery. The voltage of the DC-link is controlled using a two stage control approach. In the first stage, the required overall current to keep the voltage at its nominal reference value is calculated. In the second stage, the generated current by each power source is controlled using the output of the energy management module. The schematic diagram of the power management module is depicted in Fig. 7.

The first stage acts as an imaginary controller with which the required overall DC current to keep the DC-link voltage at its desired value is determined. Take v^*_{dc} as the desired DC voltage. Considering (6), the required current to keep the DC-link voltage around the desired value can be computed using a Proportional-Integral (PI) control scheme as:

$$i^*_{\text{dc}}(t) = K_{\text{p}}\left(v^*_{\text{dc}}(t) - v_{\text{dc}}(t)\right) + K_{\text{i}} \int_0^t \left(v^*_{\text{dc}}(\tau) - v_{\text{dc}}(\tau)\right) d\tau, \tag{47}$$

where K_{p} and K_{i} are the PI coefficients. Using (47) and the energy management module results, the reference current for different on-board power sources can be calculated as:

$$i^*_{\text{dc}_{\text{sofc}}}(t) = i^*_{\text{dc}}(t) \frac{P^*_{sofc}(t)}{P_{\text{load}}{}'(t)} i^*_{\text{dc}_{\text{ge}}}(t) = i^*_{\text{dc}}(t) \frac{P^*_{ge}(t)}{P_{\text{load}}{}'(t)} i^*_{\text{dc}_{\text{b}}}(t) = i^*_{\text{dc}}(t) - i^*_{\text{dc}_{\text{ge}}}(t) - i^*_{\text{dc}_{\text{sofc}}}(t). \tag{48}$$

The task of the converters' controllers and field voltage controller of the synchronous generator is to guarantee DC current generation with respect to the above desired values. Moreover, the governer of the engine should be controlled such that the speed of the gas engine follows the desired nominal speed ω^*_{ge}. The desired control input for SOFC and battery converters as well as gas engine and generator can be found using PI control approach similar to (47). For the low level control of converters and generator, refer to [57,7].

4. Simulation Experiment Results

In this section, the performance of the proposed approaches is evaluated. For this purpose, a dredging vessel, built by our project partner Royal IHC, is considered. The PPS, operating profiles information and data are provided by Royal IHC. The dredger has a 24 MW installed power on-board which is divided between 4 diesel-generators over two switchboards. The PPS configuration of the vessel is all-electric in which the loads are connected to power sources using an electrical network. In Fig. 8, a schematic diagram of its PPS configuration is provided.

The dredger (Fig. 8) has two switchboards for port and starboard sides which can be connected through switches and choppers. Each switchboard is connected to certain dredging and propulsive loads. Based on the proposed configuration and approaches in Sections 2 and 3, the configuration in Fig. 1 is proposed for this dredger. As a result, each bus bar connects a gas engine, a SOFC, and a battery to the loads. Moreover, the proposed PPS is a DC in which DC/DC converters are used for the battery and the SOFC. Only one bus bar is simulated in the experiments to reduce the complexity of the analysis.

To establish the simulation model, information and data about different existing electrical components are shared with us by our project partners Damen Schelde Naval Shipbuilding and Royal IHC. Some of the validation results of components are shown in Fig. 3. For the mechanical components the information and data from Wärtsilä engines are used [45]. For more information about the modeling and validation refer to [41,9].

Matlab/Simulink R2020b is used for simulations and Simscape toolbox is partially adopted for modeling of the electrical components. The simulations are carried out using a PC with 2.8 GHz Intel Core i7-7600U CPU and 8 GB RAM.

The port side PPS of the original dredger has two 6 MW diesel-generators which take in total 200 t of weight and around 150 m^3 of space [45]. For our evaluations, we use two different operating profiles of the real ship: an 8 h dredging in rock (Fig. 5 and a 10 h dredging in sand. Based on these operating profile $P_{\text{w}_{\max}} = 8.3$ MW and $P_{\max} = 12$ MW. Four scenarios are considered for the ship design. The first scenario is a retrofitting case in which no engine room size increase is allowed, i.e. $W_{\text{v}} = 200$ t and $S_{\text{v}} = 300$ m^3. In the second and the third scenarios 25% and 50% engine room size and weight increase are allowed,

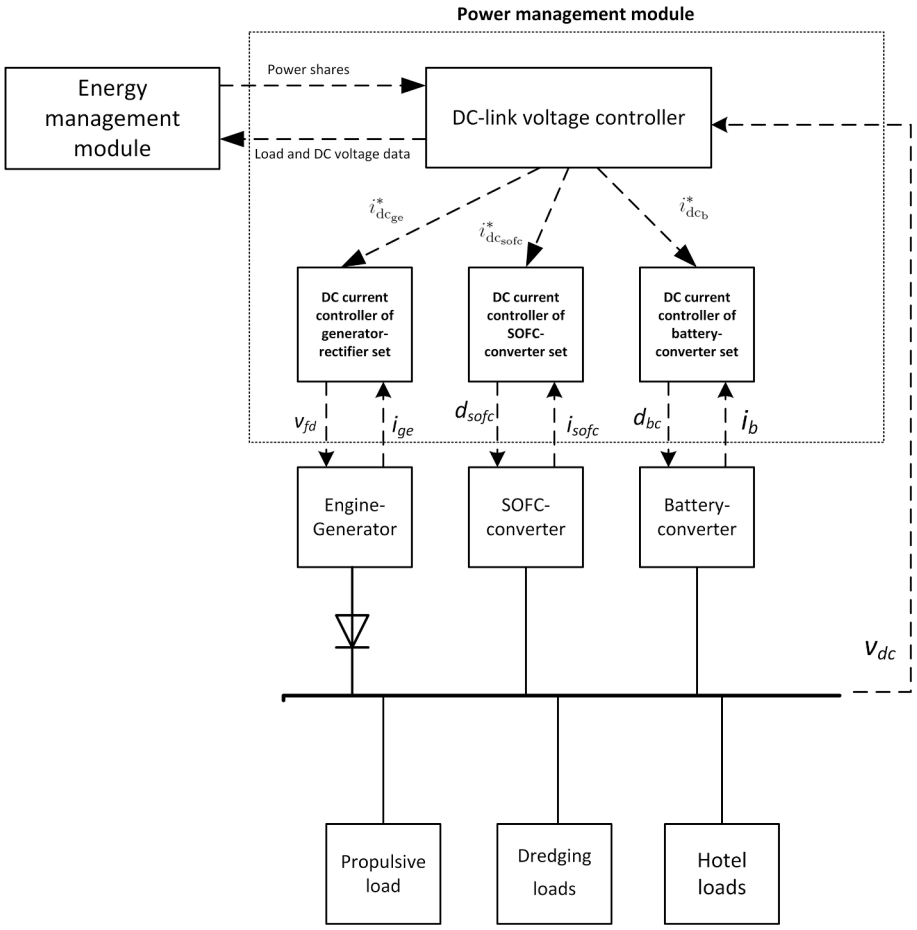

Fig. 7. Schematic diagram of the proposed power management approach.

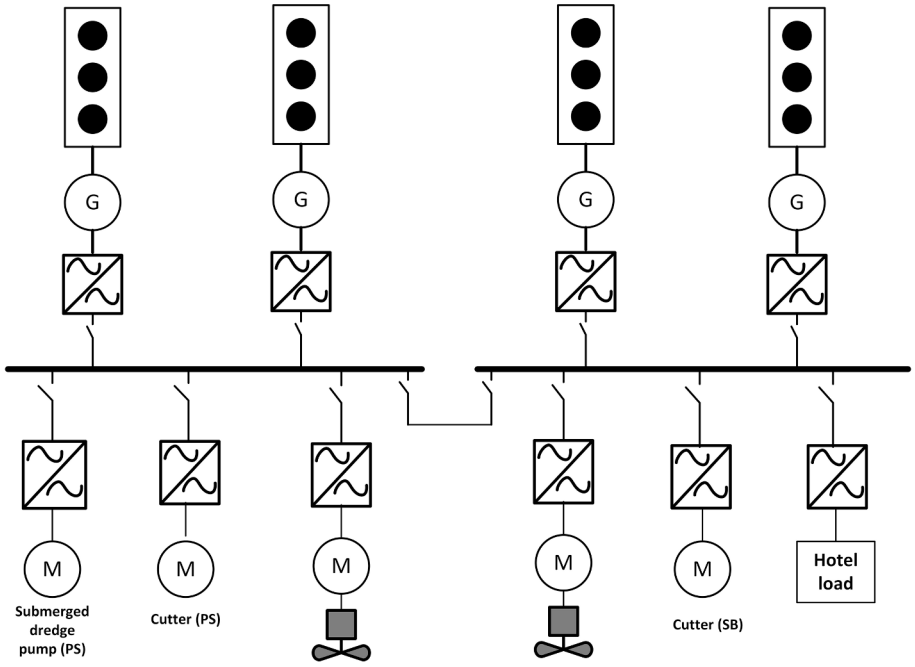

Fig. 8. Single line diagram of the vessel under study.

respectively. In Scenario 4, there is enough room for a 8.3 MW SOFC system and therefore, no power is assigned to the gas engine. The weight and space to power densities of the power sources are extracted from literature. Values for the SOFC are based on a commercially available 300 kWe platform, which is corrected upwards to account for ongoing improvements as presented in [58]. The simulation parameters for the component sizing optimization problem are given in the appendix.

The results of the component sizing optimization problem are shown in Table 1. The results show that as the space and weight limits are increased, more power is considered for the SOFC as its space and weight power densities are lower than the gas engine. Using these achieved power ratings, DC-PPS models of the dredger for these different scenarios are established.

The simulation results of the SOFC-based DC-PPS for Scenario 3 are given in Figs. 9 and 10. The DC-link voltage of the DC-PPS is shown in Fig. 9a, which stays around its nominal value and indicates the stability of power system. This verifies that the DC current generation by power sources has been carried out properly. The DC currents generated by on-board power sources are shown in Fig. 9c. The SoC of the battery is in Fig. 9b which stays between its desired range, i.e., 40% to 70%. Scenario 2 results for rock dredging are shown in Fig. 11 and 12. The operating profile is presented in Fig. 11a. The SOFC stack voltage and stable speed of the engine indicate the stability of the system in Fig. 11. The fuel consumption rate of the SOFC and the gas engine are presented in Fig. 12a. The field voltage of the synchronous generator and the torque of the gas engine are shown in Figs. 12b and 12c. The field voltage is a control input which determines how much DC current should be generated at the nominal voltage, while the inlet fuel controls the speed of the gas engine.

The simulation results of different scenarios are provided in Table 2. As it is shown, with the increase in available space, which results in higher efficiency, less fuel consumption and CO_2 emissions. As an example, the average reduction of fuel consumption is around 11% if the engine room size and weight are increased by 25% and it is 24% if the allowed size and weight increase are 50%. Switching to a fully SOFC-powered DC-PPS (Scenario 4) leads to around 30% fuel consumption reduction in comparison to Scenario 1. This is a result of shifting the power and load towards the SOFC. Note that in Scenario 1, 2, 3, and 4, the SOFC-gas engine power ratings are 17%-83%, 50%-50%, 80%-20%, and 100%-0%, respectively. Therefore, if only LNG is used on-board a 60% addition of power share towards SOFC leads to around 25% of fuel efficiency improvement and emission reduction, while a complete shift towards SOFC leads to 30% reduction. In Fig. 13 the fuel consumption reduction as a result of allowable overall size and weight increase is shown. From this figure it can be concluded that per 1% percent of size and weight increase, the fuel consumption is reduced by 0.5% in the region of 0–50% engine room size increase if the combination of the proposed approaches are used. This number is almost halved in the region of 50–70% size and weight increase.

The results of the proposed approaches are also compared with the conventional design cases. Two conventional scenarios are considered. The first one is fully diesel-electric case (Fig. 8) where the power is provided by the diesel-generators. The second scenario is a newer design where the flywheel energized dual fuel engines are adopted and the use of diesel is decreased as much as possible [40]. Therefore, the engines operate mostly in LNG mode. As a result, we neglected the use of diesel for this scenario. These results are provided in Table 2.

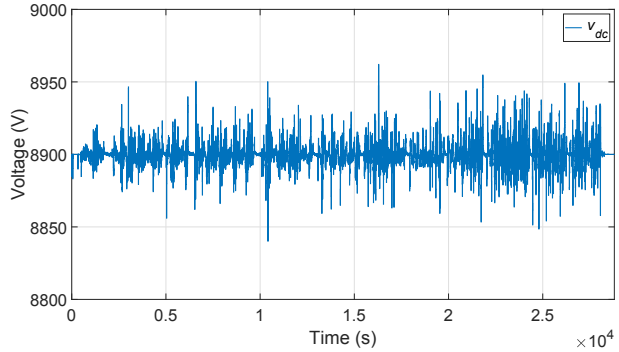

(a) DC-link voltage.

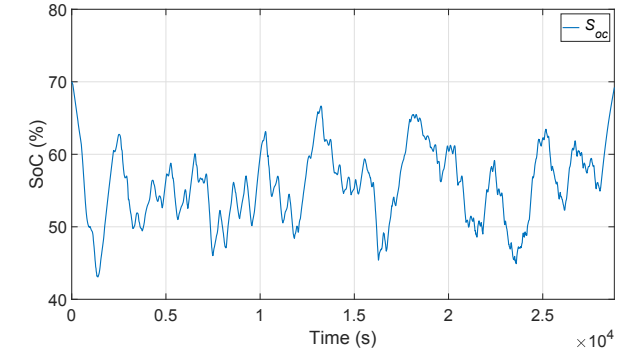

(b) SoC of the battery.

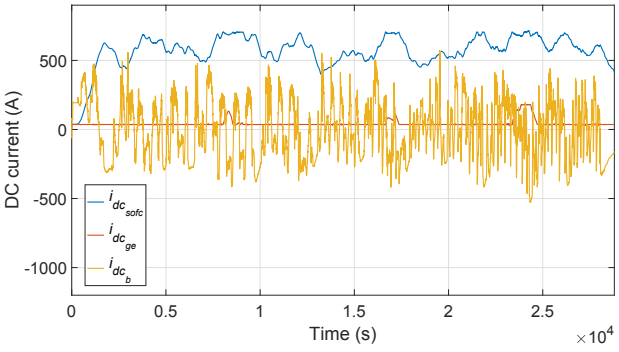

(c) Generated DC currents by sources.

Fig. 9. Simulation results of the electrical components in Scenario 3. The gas engine is mostly providing a low power as the SOFC is preferred by the energy management algorithm due to its higher efficiency.

4.1. Results and Discussion

The results show that the CO_2 reduction in the retrofitting scenario in comparison with the diesel-electric case and LNG case is around 32% and 12% respectively. The CO_2 reduction in Scenario 3 compared with

Table 1
The results of the proposed optimization-based component sizing approach for four available size and weight scenarios.

Design scenario	Maximum space (m^3) and weight (t)	SOFC power (MW)	Gas engine power (MW)	Battery size (MWh)
Scenario 1: retrofitting	$W_v = 200, S_v = 300$	1.35	7	2.8
Scenario 2: 25% increase	$W_v = 250, S_v = 375$	4.2	4.1	2.8
Scenario 3: 50% increase	$W_v = 300, S_v = 450$	6.7	1.6	2.8
Scenario 4: 70% increase	$W_v = 340, S_v = 510$	8.3	0	2.9

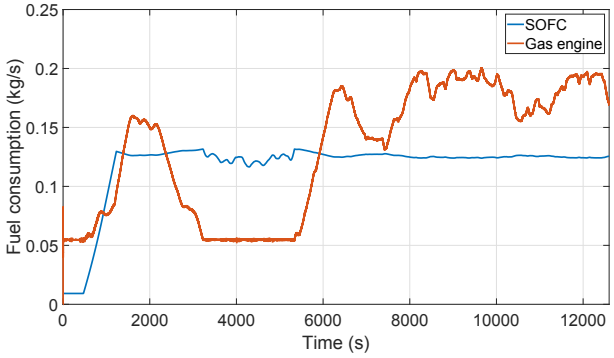

(a) Fuel consumption rate.

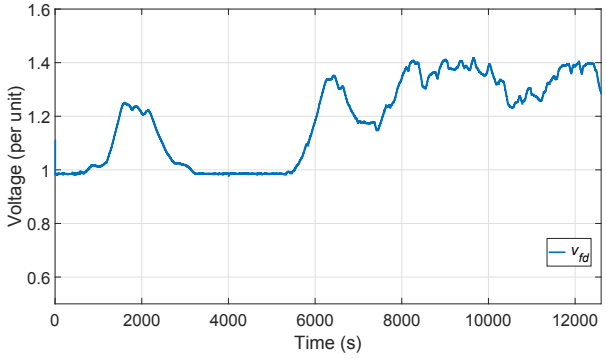

(b) Field voltage of the generator.

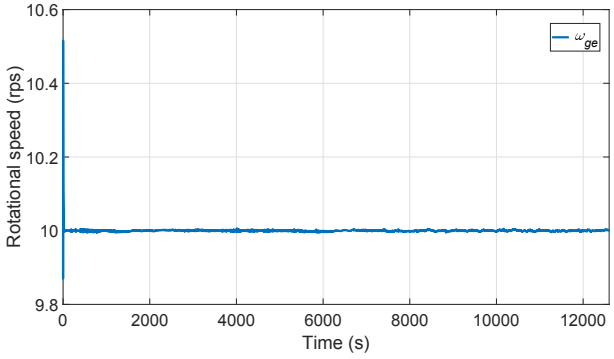

(c) Gas engine's shaft speed.

Fig. 10. Simulation results of Scenario 3 for sand dredging.

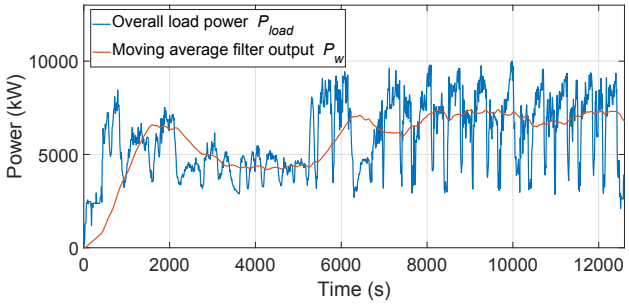

(a) Rock dredging operating profile.

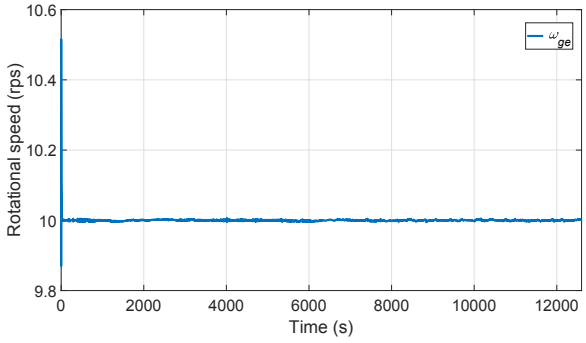

(b) Shaft speed of the gas engine.

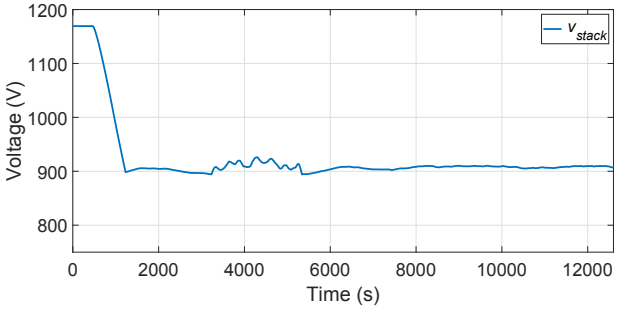

(c) Stack voltage of the SOFC.

Fig. 11. Operating profile and simulation results of Scenario 2 for rock dredging.

the conventional diesel-electric case is 49.1% and 47.5%, which satisfies the 2030 green house gas reduction goals of International Maritime Organization (IMO) [8]. In Scenario 4, where only SOFC is used, the CO_2 emissions reduction is around 53% and 39% on average in comparison with the conventional diesel and LNG cases. Considering the lower heating value of 13.8 kWh/kg and 11.8 kWh/kg for LNG and marine diesel respectively, the fuel utilization efficiency is increased by 21% on average, if the proposed approaches are used.

In Fig. 14, the effect of an increase in the SOFC power share is shown. It suggests that with every percent of SOFC share increase around 0.25% of CO_2 decrease in comparison with conventional diesel-electric scenario and 0.32% CO_2 reduction compared to the LNG scenario can be achieved. It can also be concluded that with a more than 50% SOFC power share, the 2030 IMO's CO_2 reduction goal can be achieved.

One of the main advantages of using the proposed PPS design and approaches is the potentiality for the reduction of installed power since the battery is capable of shaving the momentarily high peaks. So, for vessel types with highly fluctuating operating profiles, the installed power of non-storing sources (such as engines and fuel cells) can be reduced. In the case study of this paper, this installed power is reduced by 3.7 MW. Moreover, with the advances in the SOFC technology, the transient capabilities are expected to be improved which leads to less dependency on the battery and smaller battery size.

5. Conclusions and future research

In this paper, a new approach has been proposed to enable the use of Solid Oxide Fuel Cells (SOFC) as the main power source on-board of vessels. Liquid Natural Gas (LNG) is considered as the main and only fuel on-board. A Direct Current Power and Propulsion System (DC-PPS) is proposed for the integration of SOFCs into the vessel. First, a state space model is proposed for the power generation side of the DC-PPS and then, the component sizing, energy and power management approaches are presented. The proposed optimization-based component sizing approach determines the best power rating for the SOFC, gas engine, and the battery given the space and weight constraints. For the design of the energy management approach, a moving average filtering scheme is considered which calculates the average of the overall load over a bounded window. The size of this window is determined based on the transient capabilities of the gas engine and the SOFC. Then, through an

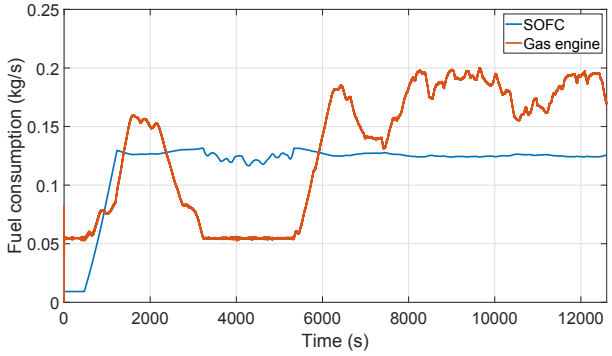

(a) Fuel consumption rate.

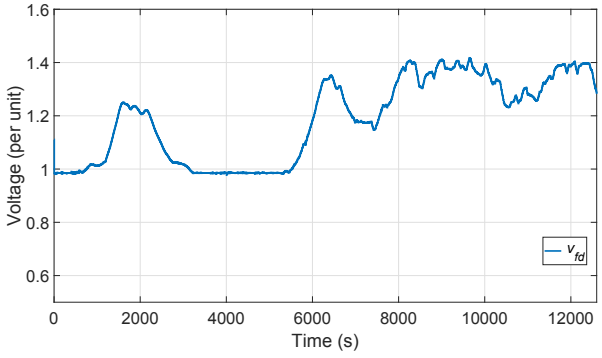

(b) Field voltage of the generator.

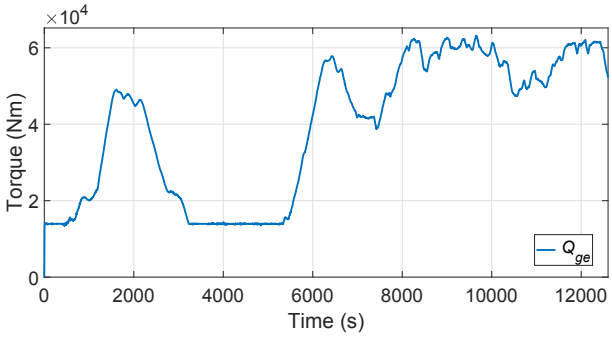

(c) Torque of the gas engine.

Fig. 12. Simulation results of Scenario 2 for rock dredging.

optimization problem, the optimal power split between different sources is computed. The power management approach, which is in harmony with the energy management scheme, controls the voltage of the DC-link, shaft speed of the gas engine, and the generated DC currents by different power sources. While the proposed component sizing scheme is used in the ship design stage, the energy and power management approaches work continuously during operation. The results suggest a large reduction in fuel consumption and emissions and increase of the efficiency depending on the SOFC power share. With an above 50% increase of the engine room's space and weight, the emission reduction goals of the International Maritime Organization (IMO) can be reached.

This paper is the first paper in the literature which enables the use of SOFCs as the main power source for vessels by proposing energy and power management approaches. The results of this paper suggest that a maximum of 53% emission reduction in comparison with the conventional designs can be achieved if LNG-fueled SOFCs are used on-board in

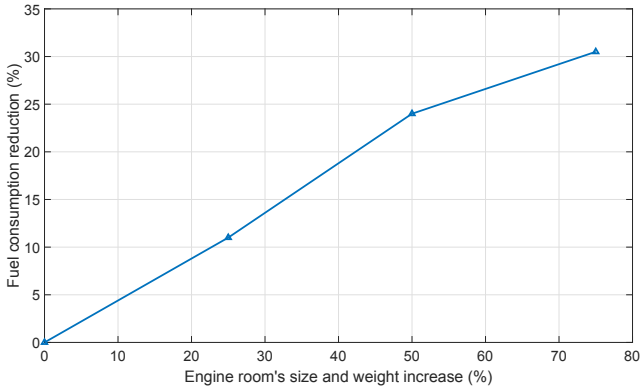

Fig. 13. Fuel consumption decrease as a result of allowable size and weight increase if the combination of proposed approaches are used.

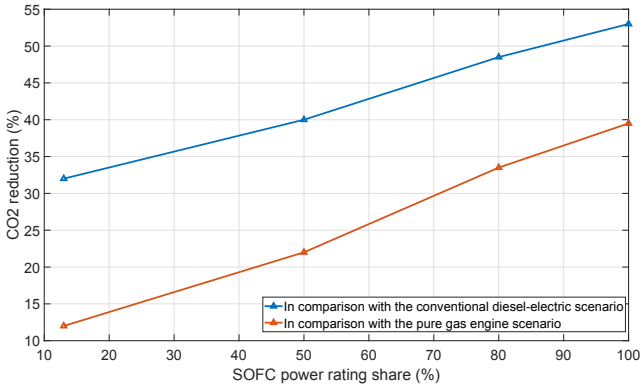

Fig. 14. CO_2 emissions reduction versus the SOFC share increase. The SOFC share increase leads to linear reduction of CO_2 with slopes of 0.25 and 0.32 in comparison with diesel and LNG scenarios, respectively.

Table 2
The results of the proposed approaches for three available size and weight scenarios versus the results from the conventional scenarios.

Design scenario	Engine consumption (kg)	SOFC consumption (kg)	Overall consumption (kg)	Overall Energy (kWh)	Final SoC (%)	Efficiency (kWh/kg)	CO_2 emissions (kg)
S1: sand	6560	1072	7632	44650	69	5.85	20988
S1: rock	3069	449	3518	20710	55	5.88	9675
S2: sand	3169	3568	6736	44070	69	6.54	18524
S2: rock	1660	1483	3142	20440	55	6.50	8641
S3: sand	699	5021	5720	43712	69	7.64	15730
S3: rock	422	2303	2726	20250	55	7.42	7497
S4: sand	–	5200	5200	43475	64	8.36	14300
S4: rock	–	2491	2491	20287	64	8.14	6850
Diesel: sand	4876 × 2	–	9752	44480	–	4.56	30920
LNG: sand	4332 × 2	–	8664	44452	–	5.12	23820
Diesel: rock	2252 × 2	–	4504	21220	–	4.71	14284
LNG: rock	2040 × 2	–	4080	21190	–	5.2	11218

combination with the proposed component sizing, energy and power management approaches. This also can result in a maximum of 83% energy generation efficiency, depending on the operating profile. Moreover, the adoption of the proposed approaches can increase the lifetime of the battery by controlling its average State of Charge (SoC) during its lifetime as well the its depth of discharge. The results of this paper can also be extended and used for other domains including automotive and sustainable power generation, as it is shown that the proposed set of approaches can deal with all sorts of operating profiles.

It should also be mentioned that an increase in the engine room size and weight leads to more required energy for the voyages and dynamic positioning operations. At the same time, higher fuel efficiency means that less fuel can be taken on-board, which results in a smaller fuel tank size and contributed to the fuel efficiency. These effects on the ship design should be studied thoroughly from naval architecture point of view for different types of vessels. Note that the case study of this paper is a dredger which does not do any major voyage during its operation.

The results of this article suggest that a shift towards the adoption of SOFCs in combination with batteries can effectively address the challenges of the maritime sector. SOFCs enable high fuel consumption reduction while producing practically no hazardous emissions, noice and vibrations. In addition, SOFCs can be configured to use a multitude of future fuels, such as hydrogen, ammonia and methanol. However, the power density, cold start and load following capabilities of SOFC systems need further improvement to reduce their impact on ship design and operation. Other important challenges are the high capital cost and limited lifetime.

Although methane (CH_4) emissions are not globally regulated, there is a need to focus on reduction of CH_4 emissions due to their significantly high global warming potential. Application of the proposed LNG-fueled hybrid power generation system can provide promising CH_4 reductions compared to an LNG-fueled only gas engine power unit. Methane reductions of 50% or higher could be achievable for the SOFC-gas engine power splits proposed in this research [26]. This is because, in the hybrid power generation system, only the gas engine contributes to methane slip. Thus, employing the SOFC as the main on-board power source will allow for significant methane emissions reductions. Furthermore, methane slip emissions from the engine can also be reduced by employing various methodologies such as zero valve overlap, hydrogen-natural gas blending, and after-treatment.

The next step to increase further the efficiency of the hybrid power generation using SOFCs is studying a novel SOFC-based power and propulsion system where the anode-off gas of the SOFC is used as a fuel for the gas engine. The aim is to propose novel design and control approaches such that the efficiency increase and emissions reduction that are proposed in this paper can be pushed even further.

CRediT authorship contribution statement

Ali Haseltalab: Conceptualization, Methodology, Validation, Formal analysis, Investigation, Writing - original draft. **Lindert van Biert:** Conceptualization, Validation, Formal analysis, Investigation, Writing - original draft. **Harsh Sapra:** Conceptualization, Formal analysis, Writing - review & editing. **Benny Mestemaker:** Data curation, Validation, Writing - review & editing. **Rudy R. Negenborn:** Supervision, Project administration, Funding acquisition, Writing - review & editing.

Declaration of competing interest

The authors declare that they have no known competing financial interests or personal relationships that could have appeared to influence the work reported in this paper.

Acknowledgment

This research is supported by the project *"GasDrive: Minimizing emissions and energy losses at sea with LNG combined prime movers, underwater exhausts and nano hull materials"* (project 14504) of the Netherlands Organization for Scientific Research (NWO), domain Applied and Engineering Sciences (TTW) and the Researchlab Autonomous Shipping (RAS) at Delft University of Technology.

Appendix A

A.1. DC-PPS component sizing values

- **Density specs:** $d_{w_{sofc}} = 30$ t/MW, $d_{w_{ge}} = 15$ t/MW, $d_{w_b} = 20$ t/MW, $d_{s_{sofc}} = 50$ m^3/MW, $d_{s_{ge}} = 20$ m^3/MW, $d_{s_b} = 30$ m^3/MW.
- **Efficiency specs:** $\eta_{\max_{sofc}} = 0.036$ g/kJ, $\eta_{\max_{ge}} = 0.048$ g/kJ, $\eta_{\max_b} = 0.070$ g/kJ, $C_{\text{rate}_{\max}} = 3$.
- **Transients specs:** $T_{\text{rise}_{\text{sofc}}} = 880$ s, $T_{\text{rise}_{\text{ge}}} = 300$ s.

A.2. SOFC design values

- **Thermodynamic properties (800°C):** $\Delta\overline{h}_{\text{f}} = 789.2$kJ mol^{-1}, $\Delta\overline{g}_{\text{f}} = 789.2$kJ mol^{-1} K^{-1}, $\overline{R} = 8.314$ J mol^{-1}K^{-1}, $F = 96485$ C mol^{-1}.
- **Physical properties:** $\tau_{\text{an}} = 500e^{-6}$ m, $\tau_{\text{ca}} = 50e^{-6}$ m, $\tau_{\text{el}} = 20e^{-6}$ m, $\sigma_{\text{an}} = 8e^4\ \Omega^{-1}$ m^{-1}, $\sigma_{\text{ca}} = 8.4e^4\ \Omega^{-1}$ m^{-1}, $\sigma_{\text{el}} = 2.26\ \Omega^{-1}$ m^{--1}.
- **Electrochemical properties:** $u_{\text{f}} = 0.85, D_{\text{eff,an}} = 3.66e^{-5}$ m^2 s^{--1}, $D_{\text{eff,ca}} = 1.37e^{-5}$ m^2 s^{--1}, $j_{0,\text{an}} = 4.64e^3\ \Omega^{-1}$ m^{-2}, $j_{0,\text{ca}} = 2.33e^3\ \Omega^{-1}$ m^{--2}, $\omega = 0.5, v_{\text{cell}}^{\text{design}} = 0.7$ V.

A.3. Scenario 1

- **Gas Engine:** $K_{\text{en}} = 111610$, six cylinders, 7 MW, engine-generator gear ratio: $\frac{1}{6}, a_{\text{ge}} = -8.293e-08, b_{\text{ge}} = 0.04399, c_{\text{ge}} = 30.79$.
- **SOFC:** 1.35 MW $n_{\text{series}} = 1200, P_{\text{loss,ld}} = 0.025, P_{\text{loss,c}} = 0.025, \tau_{\text{SOFC}} = \frac{1}{900}$ s^{-1},$a_{\text{sofc}} = 8.582e-06, b_{\text{sofc}} = 0.02423, c_{\text{sofc}} = 1.238$.
- **Synchronous generator:** 6.850 MW, 6600 v, 60 Hz, 10 poles, $H = 0.71, r_s = 0.0343, r_{\text{fd}} = 0.2, r_{\text{kd}} = 0.702, r_{\text{kq}} = 0.1032, L_{\text{d}} = 0.031, L_{\text{md}} = 0.0290, L_{\text{kd}} = 0.0311, L_{\text{fd}} = 0.4620, L_{\text{q}} = 0.0153, L_{\text{mq}} = 0.0164$ and $L_{\text{kq}} = 0.0167$. Resistance values are in ohm and inductance values are in Henry.

A.4. Scenario 2

- **Gas Engine:** $K_{\text{ge}} = 684400$, six cylinders, 4.1 MW, engine-generator gear ratio: $\frac{1}{6}, a_{\text{ge}} = -1.444e-07, b_{\text{ge}} = 0.04487, c_{\text{ge}} = 18.4$.

- **SOFC:** 4.2 MW, $n_{\text{series}} = 1200, P_{\text{loss,ld}} = 0.025, P_{\text{loss,c}} = 0.025, \tau_{\text{SOFC}} = \frac{1}{900}\,\text{s}^{-1}$, $a_{\text{sofc}} = 2.759e-06, b_{\text{sofc}} = 0.02423, c_{\text{sofc}} = 3.851$.
- **Synchronous generator:** 4.05 MW, 6600 v, 60 Hz, 10 poles, $H = 0.56, r_s = 0.0550, r_{\text{fd}} = 0.2, r_{\text{kd}} = 1.5049, r_{\text{kq}} = 0.1706, L_{\text{d}} = 0.05168, L_{\text{md}} = 0.05107, L_{\text{kd}} = 0.0600, L_{\text{fd}} = 0.310, L_{\text{q}} = 0.02702, L_{\text{mq}} = 0.0122$ and $L_{\text{kq}} = 0.02041$. Resistance values are in ohm and inductance values are in Henry.

A.5. Scenario 3

- **Gas Engine:** $K_{\text{ge}} = 254652$, six cylinders, 1.6 MW, engine-generator gear ratio: $\frac{1}{6}, a_{\text{ge}} = -3.879e-07, b_{\text{ge}} = 0.04621, c_{\text{ge}} = 7.381$.
- **SOFC:** 6.7 MW, $n_{\text{series}} = 1200, P_{\text{loss,ld}} = 0.025, P_{\text{loss,c}} = 0.025, \tau_{\text{SOFC}} = \frac{1}{900}\,\text{s}^{--1}$, $a_{\text{sofc}} = 1.729e-06, b_{\text{sofc}} = 0.02423, c_{\text{sofc}} = 6.143$.
- **Synchronous generator:** 1.55 MW, 6600 v, 60 Hz, 10 poles, $H = 0.46, r_s = 0.0740, r_{\text{fd}} = 0.18, r_{\text{kd}} = 1.9067, r_{\text{kq}} = 0.2306, L_{\text{d}} = 0.08828, L_{\text{md}} = 0.09100, L_{\text{kd}} = 0.0910, L_{\text{fd}} = 0.510, L_{\text{q}} = 0.0470, L_{\text{mq}} = 0.0180$ and $L_{\text{kq}} = 0.0306$. Resistance values are in ohm and inductance values are in Henry.

A.6. Scenario 4

- **SOFC:** 8.3 MW, $n_{\text{series}} = 1200, P_{\text{loss,ld}} = 0.025, P_{\text{loss,c}} = 0.025, \tau_{\text{SOFC}} = \frac{1}{900}\,\text{s}^{-1}$, $a_{\text{sofc}} = 1.396e-06, b_{\text{sofc}} = 0.02423, c_{\text{sofc}} = 7.61$.

A.7. Electrical components

- **Rectifier:** Six-pulse rectifier, efficiency factor: 98.1%.
- **DC-link:** $C = 1$ F.
- **Converter:** $L = 0.0005$H.
- **Battery:** $v_{\text{b}} = 500$V, $r_{\text{b}} = 0.0125$.

A.8. CO_2 calculation

- For diesel engine, assuming operation on F76 marine fuel with 86.5% mass fraction of carbon yields to 3.171 kg CO_2 per kilogram fuel.
- For the LNG-based scenarios, assuming operation on 100% methane, the CO_2 emissions yields to 2.75 kg per kilogram LNG.

References

[1] Brynolf S, Taljegard M, Grahn M, Hansson J. Electrofuels for the transport sector: A review of production costs 81 1887–1905. doi: 10.1016/j.rser.2017.05.288. URL https://www.sciencedirect.com/science/article/pii/S1364032117309358.

[2] Burel F, Taccani R, Zuliani N. Improving sustainability of maritime transport through utilization of liquefied natural gas (lng) for propulsion 57 412–420. doi: 10.1016/j.energy.2013.05.002. URL https://www.sciencedirect.com/science/article/pii/S0360544213003861.

[3] van Biert L, Godjevac M, Visser K, Aravind P. A review of fuel cell systems for maritime applications 327 345–364. doi: 10.1016/j.jpowsour.2016.07.007. URL https://www.sciencedirect.com/science/article/pii/S0378775316308631.

[4] Ma S, Lin M, Lin TE, Lan T, Liao X, MarTchal F, et al. Fuel cell-battery hybrid systems for mobility and off-grid applications: A review 135 110119. doi: 10.1016/j.rser.2020.110119. URL https://www.sciencedirect.com/science/article/pii/S136403212030410X.

[5] Haseltalab A, van Biert L, Mestemaker B, Negenborn RR. Energy management for hybrid power generation using solid oxide fuel cell, Zenodo. doi:10.24868/issn.2631-8741.2020.006. URL https://doi.org/10.24868/issn.2631-8741.2020.006.

[6] Haseltalab A, Negenborn RR. Model predictive maneuvering control and energy management for all-electric autonomous ships. Appl Energy 2019;251:113308. https://doi.org/10.1016/j.apenergy.2019.113308. URL http://www.sciencedirect.com/science/article/pii/S0306261919309705.

[7] Zahedi B, Norum L. Modeling and simulation of all-electric ships with low-voltage dc hybrid power systems. IEEE Trans Power Electron 2013;28(10):4525–37. https://doi.org/10.1109/TPEL.2012.2231884.

[8] IMO, International convention for the prevention of pollution from ships (marpol) (2011). http://www.imo.org/en/About/Conventions/ListOfConventions/Pages/International-Convention-for-the-Prevention-of-Pollution-from-Ships-(MARPOL).aspx.

[9] van Biert L. Solid oxide fuel cells for ships: System integration concepts with reforming and thermal cycles. doi:10.4233/uuid:dd1f7899-38ee-4c78-a5b0-a6fa92c90f56.

[10] Baldi F, Moret S, Tammi K, MarTchal F. The role of solid oxide fuel cells in future ship energy systems 194 116811. doi: 10.1016/j.energy.2019.116811. https://www.sciencedirect.com/science/article/pii/S036054421932506X.

[11] Project ishy: Implementation of ship hybridisation. https://www.interreg2seas.eu/nl/ISHY.

[12] Tse LKC, Wilkins S, Martinez-Botas RF. Dynamic modelling of a SOFC-GT hybrid system for transport applications, in: European Ele-Drive Conference Brussels, Belgium, 2007.

[13] METHAPU prototypes methanol SOFC for ships, Fuel Cells Bulletin 2008 (5) (2008) 4 – 5.

[14] Rechberger J, Schauperl R, Hansen JB, Larsen PK. Development of a methanol SOFC APU demonstration system. ECS Trans 2009;25(2):1085–92.

[15] Strazza C. Del Borghi A, Costamagna P, Traverso A, Santin M. Comparative LCA of methanol-fuelled SOFCs as auxiliary power systems on-board ships 87 (5) 1670–1678.

[16] Díaz-de Baldasano MC, Mateos FJ, Núñez-Rivas LR, Leo TJ. Conceptual design of offshore platform supply vessel based on hybrid diesel generator-fuel cell power plant 116 91–100.

[17] Rechberger J, Schauperl R, Hansen JB, Larsen PK. Development of a methanol SOFC APU demonstration system 25 (2) 1085–1092. doi:10.1149/1.3205635.

[18] Strazza C, Borghi AD, Costamagna P, Traverso A, Santin M. Comparative LCA of methanol-fuelled SOFCs as auxiliary power systems on-board ships 87 (5) 1670–1678. doi:10.1016/j.apenergy.2009.10.012.

[19] Nehter P, Wildrath B, Bauschulte A, Leites K. Diesel based SOFC demonstrator for maritime applications. ECS Trans 2017;78(1):171–80.

[20] Huerta GV, Jordán JÁ, Marquardt T, Dragon M, Leites K, Kabelac S. Exergy analysis of the diesel pre-reforming SOFC-system with anode off-gas recycling in the SchIBZ project, Part II: System exergetic evaluation. Int J Hydr Energy 2019;44(21):10916–24.

[21] Ghezel-Ayagh H, Jolly S, Sanderson R, Hunt J, Davis KE, Lukas M, et al. Hybrid SOFC-battery power system for large displacement unmanned underwater vehicles 51 (1) 95–101. doi:10.1149/05101.0095ecst.

[22] Ghezel-Ayagh H, Junker ST, Peters JA, Miller TF, Martin JD, Lowe D. Development of solid oxide fuel cell power systems for underwater applications 12 (1) 707–711. doi:10.1149/1.2921596.

[23] Dziurdzia B, Magonski Z, Jankowski H. Commercialisation of solid oxide fuel cells - opportunities and forecasts 104 012020. doi:10.1088/1757-899x/104/1/012020.

[24] Ezgi C, Çoban MT. +zgnn Selvi, Design and thermodynamic analysis of an SOFC system for naval surface ship application 10 (3). doi:10.1115/1.4024254.

[25] Wu Z, Zhu P, Yao J, Tan P, Xu H, Chen B, et al. Dynamic modeling and operation strategy of natural gas fueled SOFC-engine hybrid power system with hydrogen addition by metal hydride for vehicle applications 5 100074. doi:10.1016/j.etran.2020.100074.

[26] Sapra H, Stam J, Reurings J, van Biert L, van Sluijs W, de Vos P, et al. Integration of solid oxide fuel cell and internal combustion engine for maritime applications 281 115854. doi:10.1016/j.apenergy.2020.115854.

[27] de Baldasano MCD, Mateos FJ, Núñez-Rivas LR, Leo TJ. Conceptual design of offshore platform supply vessel based on hybrid diesel generator-fuel cell power plant 116 91–100. doi:10.1016/j.apenergy.2013.11.049.

[28] Ahn J, Park SH, Noh Y, Choi BI, Ryu J, Chang D, et al.s Performance and availability of a marine generator-solid oxide fuel cell-gas turbine hybrid system in a very large ethane carrier 399 199–206. doi:10.1016/j.jpowsour.2018.07.103.

[29] Jia Z, Sun J, Dobbs H, King J. Feasibility study of solid oxide fuel cell engines integrated with sprinter gas turbines: Modeling, design and control 275 111–125. doi:10.1016/j.jpowsour.2014.10.203.

[30] Geertsma R, Negenborn R, Visser K, Loonstijn M, Hopman J. Pitch control for ships with diesel mechanical and hybrid propulsion: Modelling, validation and performance quantification. Appl Energy 2017;206:1609–31. https://doi.org/10.1016/j.apenergy.2017.09.103. URL http://www.sciencedirect.com/science/article/pii/S0306261917313855.
[31] Hou J, Song Z, Hofmann H, Sun J. Adaptive model predictive control for hybrid energy storage energy management in all-electric ship microgrids. Energy Convers Manage 2019;198:111929. https://doi.org/10.1016/j.enconman.2019.111929. URL http://www.sciencedirect.com/science/article/pii/S0196890419309203.
[32] Geertsma R, Negenborn R, Visser K, Hopman J. Design and control of hybrid power and propulsion systems for smart ships: A review of developments. Appl Energy 2017;194:30–54. https://doi.org/10.1016/j.apenergy.2017.02.060. URL http://www.sciencedirect.com/science/article/pii/S0306261917301940.
[33] Kalikatzarakis M, Geertsma R, Boonen E, Visser K, Negenborn R. Ship energy management for hybrid propulsion and power supply with shore charging 76 133–154. doi:10.1016/j.conengprac.2018.04.009.
[34] Bassam AM, Phillips AB, Turnock SR, Wilson PA. Development of a multi-scheme energy management strategy for a hybrid fuel cell driven passenger ship 42 (1) 623–635. doi:10.1016/j.ijhydene.2016.08.209.
[35] Wu P, Partridge J, Bucknall R. Cost-effective reinforcement learning energy management for plug-in hybrid fuel cell and battery ships 275 115258. doi:10.1016/j.apenergy.2020.115258.
[36] Hasanvand S, Rafiei M, Gheisarnejad M, Khooban MH. Reliable power scheduling of an emission-free ship: Multiobjective deep reinforcement learning 6 (2) 832–843. doi:10.1109/tte.2020.2983247.
[37] Chen H, Zhang Z, Guan C, Gao H. Optimization of sizing and frequency control in battery/supercapacitor hybrid energy storage system for fuel cell ship 197 117285. doi:10.1016/j.energy.2020.117285.
[38] Jokela T, Iraklis A, Kim B, Gao B. Combined sizing and EMS optimization of fuel-cell hybrid powertrains for commercial vehicles, in: SAE Technical Paper Series, SAE International. doi:10.4271/2019-01-0387.
[39] Barelli L, Bidini G, Ciupăgeanu D, Pianese C, Polverino P, Sorrentino M. Stochastic power management approach for a hybrid solid oxide fuel cell/battery auxiliary power unit for heavy duty vehicle applications 221 113197. doi:10.1016/j.enconman.2020.113197.
[40] Mestemaker B, Castro MG, van den Heuvel H, Visser K. Dynamic simulation of a vessel drive system with dual fuel engines and energy storage, Energy 194 (2020) 116792. doi:https://doi.org/10.1016/j.energy.2019.116792. URL http://www.sciencedirect.com/science/article/pii/S0360544219324879.
[41] Haseltalab A. Control for autonomous all-electric ships, Ph.D. thesis, Delft University of Technology (2019).
[42] Izadi-Zamanabadi R, Blanke M. A ship propulsion system as a benchmark for fault-tolerant control. Control Eng Pract 1999;7(2):227–39. https://doi.org/10.1016/S0967-0661(98)00149-X. URL http://www.sciencedirect.com/science/article/pii/S096706619800149X.
[43] Grimmelius PSD, Schulten HT. The use of diesel engine simulation models in ship propulsion plant design and operation, in: CIMAC, 2007, 2007.
[44] Blanke M, Andersen J. On Dynamics of Large Two Stroke Diesel Engines. New Res Identif 1984.
[45] Wartsila engines. https://www.wartsila.com/marine/build/engines-and-generating-sets/.
[46] Krause SDSPC, Wasynczuk O, Pekarek S. Analysis of Electric Machinery and Drive Systems. 3rd Edition. Wiley; 2013.
[47] Plett GL. Extended kalman filtering for battery management systems of lipb-based hev battery packs: Part 1. background, Journal of Power Sources 134 (2) (2004) 252–261. doi: 10.1016/j.jpowsour.2004.02.031. http://www.sciencedirect.com/science/article/pii/S0378775304003593.
[48] Ahmed K, Föger K. Perspectives in solid oxide fuel cell-based microcombined heat and power systems. J Electrochem Energy Convers Storage 2017;14(3):031005.
[49] van Biert L, Visser K, Aravind P. A comparison of steam reforming concepts in solid oxide fuel cell systems. Appl Energy 2020;264:114748.
[50] van Biert L, Woudstra T, Godjevac M, Visser K, Aravind PV. A thermodynamic comparison of solid oxide fuel cell-combined cycles. J Power Sources 2018;397:382–96.
[51] Aguiar P, Adjiman C, Brandon NP. Anode-supported intermediate temperature direct internal reforming solid oxide fuel cell. I: model-based steady-state performance 138 (1) 120–136.
[52] Staxera GmbH (D). Technical Documentation Integrated Stack Module (ISM), Technical report available at the web site http://www.fuelcellmarkets.com/content/images/articles/00864_AS_Dokumentation_ISM.pdf, accessed: 2018-10-09 (2010).
[53] Jiang J, Shi W, Zheng J, Zuo P, Xiao J, Chen X, Xu W, Zhang J-G. Optimized operating range for large-format lifepo4/graphite batteries. J Electrochem Soc 2013;161:A336–41. https://doi.org/10.1149/2.052403jes.
[54] Boveri A, Silvestro F, Molinas M, Skjong E. Optimal sizing of energy storage systems for shipboard applications. IEEE Trans Energy Convers 2019;34(2):801–11. https://doi.org/10.1109/TEC.2018.2882147.
[55] ten Cate Hoedemaker S. An assessment of the relationship between battery size, charging strategy and battery lifetime, Master's thesis.
[56] Meng L, Shafiee Q, Trecate GF, Karimi H, Fulwani D, Lu X, Guerrero JM. Review on control of dc microgrids and multiple microgrid clusters. IEEE J Emerg Select Top Power Electron 2017;5(3):928–48. https://doi.org/10.1109/JESTPE.2017.2690219.
[57] Haseltalab A, Botto MA, Negenborn RR. Model predictive dc voltage control for all-electric ships. Control Eng Pract 2019;90:133–47. https://doi.org/10.1016/j.conengprac.2019.06.018. URL http://www.sciencedirect.com/science/article/pii/S0967066119300929.
[58] Azizi A, Ahrend P, Samuelsen S, Brouwer J, et al. Prototype design and evaluation of hybrid solid oxide fuel cell gas turbine systems for use in locomotives, Tech. rep., United States. Department of Transportation. Federal Railroad Administration (2019).